Norwegian University
of Life Sciences

Master's Thesis 2016 30 ECTS
Faculty of Science and Technology

Ray Dynamics in Array of Disks investigating Light Management in Thin-Film Solar Cells

Kristian Frafjord
Environmental Physics and Renewable Energy

Acknowledgment

This thesis concludes my Master's degree in Environmental Physics and Renewable Energy at the Norwegian University of Life Sciences.

I would like to thank the following persons for being a great help during the process of finishing this thesis.

A big thanks to my supervisor, Professor Achim Kohler for his guidance and advice during this thesis. I also highly appreciate the help from Maren Anna Brandsrud who set aside her own time to support me through these months.

I am very grateful for the motivation and friendship of my fellow students through the years at NMBU and especially the last few months. A special mention to Lisa Karlsen for proofreading this thesis.

Ås, May 15, 2017

Kristian Frafjord

Abstract

The use of resonant dielectric structures have shown promising signs as a contributor of light trapping. Nanospheres as a dielectric texture on thin-film solar cells have been demonstrated to increase the overall efficiency significantly compared to flat film cells with reflection coating only. In order to better understand the rationale behind the light trapping of the nanostructure which leads to the increase in efficiency of the solar cell, it is essential to further optimise this efficiency. This thesis introduces a two-dimensional array of disks system representing a simplified model of the nanosphere structures. Simulations of the ray dynamics in the array of disks are done in order to investigate the light trapping properties of the structures. It was found that a broad spectrum of rays form stable islands of different sizes in the phase space of this system. The size of the islands represent the number of rays stabilising in this array of disks over time, and was demonstrated to depend on the refractive index of the disks as well as the distance between them.

Sammendrag

Bruk av dielektriske nanosfærer som struktur på solceller har vist lovende tegn. Tynnfilm solceller strukturert med nanosfærer har vist signifikant økt effektivitet i forhold til solceller med vanlig antireflekslag. Å forstå de grunnleggende effektene bak lysfangingen som fører til den økte absorpsjonen i solcellene bedre, er av stor betydning for videre optimalisering av effektiviteten til solceller. Denne oppgaven introduserer en streng av to-dimensjonale disker som en forenklet modell av nanostrukturene. I dette systemet ble mengder av forskjellige lysstråler simulert for å undersøke lysfangingsegenskapene i dette systemet. Simuleringene viste at en mengde av lysstrålene lagde stabile øyer i faserommet. Disse øyene var av forskjellig størrelse og avhengig av brytningsindeksen til diskene samt avstanden mellom diskene.

Contents

1. Introduction

The decline of fossil fuels and an increasing focus on environment and climate changes has seen the rise of new renewable energy. Solar cells have had a rapid growth with 50 GW of new installed capacity in 2015, which is an increase of 25% from the preceding year [11]. That was the highest increase of any renewable technology in 2015 [15]. A main driver of this growth is the rapid reduction in module prices [10]. This makes them more competitive with other power sources economically. Thin-film solar cells have been a big contributor to lower the module prices.

Thin-film solar cells are a compromise between lower price and lower efficiency. Lower prices are due to much easier fabrication of the cells and less use of material [17]. The loss in efficiency is caused by the fact that the cells are thinner than traditional, crystalline solar cells. Since for thin-film solar cells, light absorption is proportional to the film thickness [6], thinner cells transmit more light, thus the efficiency is reduced. Because of the low prices, increasing the efficiency of these cells can therefore be a big step forward for the solar industry.

Employing the ray picture of light, a way to increase the efficiency of the solar cells is to trap the light in the solar cell. This addresses a main problem in thin-film solar cells, since light rays travel in average a shorter distance in the solar cells. Normally, light trapping is achieved by changing the angle of the incident radiation [9]. This means that, instead of travelling the shortest way through the cell, it travels diagonally in the solar cell material. Thus the rays emerging from the sun travel a longer distance through the cell to increase absorption. Increasing the path length of rays in solar cells is commonly achieved by adding a textured layer on the front surface of the solar cell. Additionally, the use of a reflective back surface increases the travel length of the ray through the cell even further. Other more advanced light

trapping techniques that exist, are the use of geometric nanostructures such as wires [12], domes [22] and spheres [7]. Each of these nanostructures may have their own properties to increase the efficiency of solar cells. Understanding the rationale behind the light-trapping of nanostructures, which leads to an increase of light absorption in solar cells, is essential for maximising the efficiency of solar cells further. Using a nanosphere structure to texture solar cells has been shown to increase the efficiency of solar cells significantly compared to a flat film cell with anti-reflection coating only [7]. Furthermore, such a texture also reduces the sensitivity of various incident angles of illumination compared to a flat film solar cell [6].

The effects contributing to the increased efficiency of the solar cells has already been analysed in literature [5]. The dielectric spheres were found to increase light absorption in the photovoltaics due to different effects. Besides increased light trapping, coupling of light originating from whispering gallery modes in the spheres, can contribute to increased light absorption. Thus, an increased overall efficiency of the solar cells [7]. In order to better understand the synergy between the nanospheres and the absorbing layer that leads to increased efficiency in the solar cells, the ray dynamics in a system of disks is studied in the thesis at hand.

Chapter 2 introduces an array of disks system and uses ray dynamics to simulate the rays' trajectories through the system of disks. This is the simplest model to investigate the trapping of light in an infinite periodic structure consisting of spheres in two dimensions. The system is considered in two dimensions in order to make the investigation of the classical phase space simpler. The use of ray dynamics has its advantages. As a simplified system, it is possible to simulate the behaviour of the rays over time as it travels through many disks. Furthermore, analysis of a simple classical approach may, through a deeper understanding of the system, elucidate some of the quantum effects that arise. This is especially relevant in systems related to photovoltaics as they contain energy converting material.

To better understand the behaviour of the rays, a structural approach is made, that first examines the behaviour of single rays as the initial conditions and system parameters change. Later, trajectories of many rays are studied in phase space in order to get an overview of the light trapping abilities of the array of disks when a broad spectrum of rays approach the disks differently. For photovoltaics with nanostructures in practice, the incident light consists of many different rays and enters the system to illuminate the entire spheres. Additionally, light

approaches with changing angles throughout the day and year. However, by breaking down the complex structure of many rays approaching from different angles and positions, patterns of the dependence on system and ray parameters may become obvious. In addition, a better understanding of the dependence on initial conditions and system parameters are essential in order to optimise the structures to trap a larger fraction of light.

The efficiency of the trapping of rays is reliant on the range of different rays that can be trapped in the system. Therefore, the goal of the ray dynamics is to investigate what extent the rays can stabilise in the system. That is how big of an area in the phase space that consists of rays which are trapped in the system. The results of the simulations and the following analysis are presented in chapter 3.

2. Ray dynamics for a two dimensional system

2.1 Classical ray dynamics

Fermat's principle of least time states that a ray of light travelling between two points in a medium with a constant refractive index follows the path that takes the least time [19]. In other words, it travels in a straight line between the points in a medium of constant refractive index. When a ray approaches an interface between media of different refractive indices, it is either transmitted, reflected or both. The transmitted wave is bent according to Snell's law of refraction, Eq. 2.1, [19].

$$n_0 \cdot sin(\theta_0) = n_1 \cdot sin(\theta_1) \tag{2.1}$$

where n_0 and n_1 are the refractive indices of the corresponding media. θ_0 and θ_1 are the angles in and out of the interface respectively with regard to the normal, see Fig. 2.1. Therefore, the change in the angle of the ray depends on the magnitude of the refractive indices. This bending is called *refraction*. The reflected ray bounces off the surface with the same angle θ_0.

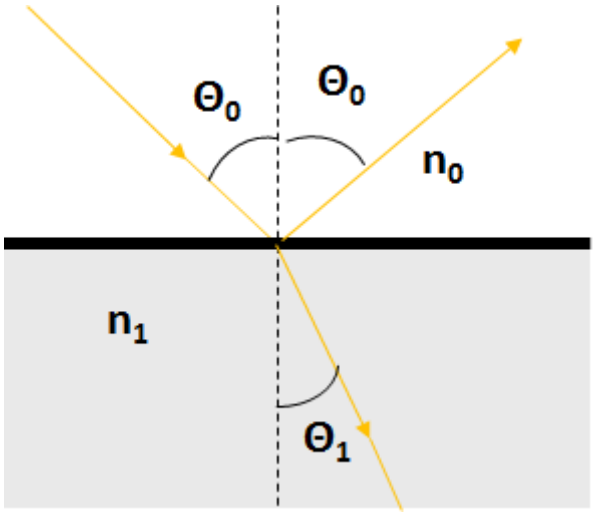

Figure 2.1: A ray approaches an interface between two different media with refractive index n_0 and n_1. The angle is refracted from the incident angle θ_0 to the outgoing θ_1

When a ray approaches an interface with a medium of lower refractive index, *total internal reflection* may have to be considered. Total internal reflection occurs when the incident angle is above a critical angle, θ_c given by Eq. 2.2 [19]. If this happens, Snell's law cannot mathematically be satisfied as $sin^{-1}\theta$ is not defined for values of θ above 1. For angles below θ_c, the ray is refracted as normal with a reflected component. However, if the angle is larger, the ray is completely reflected.

$$\theta_c = \frac{n_1}{n_0} \tag{2.2}$$

n_0 and n_1 are the refractive indices where $n_0 > n_1$.

2.2 Ray dynamics in array of disks

The model system that is considered in this thesis consists of an infinite array of disks as in Fig. 2.2. This is a two-dimensional system of closely packed disks arranged in an infinite array. The disks all have the same radius, r, and refractive index n_1. The refractive index of the surrounding medium is denoted by n_1. The path of a ray is determined by the parameters p, s and the refractive indices. The parameter p represents the momentum of the ray, while s represents the arc length from the point $s = 0$, indicated on Fig. 2.2. The system is limited

to only disks of equal size. Furthermore, it is also limited to tracing of the transmitted components of the ray. If the incident angle is below some critical angle for total reflection, ray splitting at the boundary of the disks occur. Ray splitting leads to an exponential increase of the number of rays with respect to the bounces at disk boundaries. After n bounces of a ray at a boundary, 2^n trajectories exit in the system. For simplicity, this thesis considers only the transmitted ray.

The coordinate system used for this disk model is building on the one introduced by Berry [2]. The coordinate s represents the arc length of the top half of the disk from the point $s = 0$ as indicated in Fig. 2.2. This value is normalised so that it refers to a fraction of the total arc length. Thus, it ranges from 0 to 1.

$$s = \frac{\text{arc length}}{\text{total length of the half disk}} \tag{2.3}$$

The coordinate, p, is the momentum given by,

$$p = sin(\theta), \tag{2.4}$$

where θ is the incident angle in reference to the normal of the disk at this point.

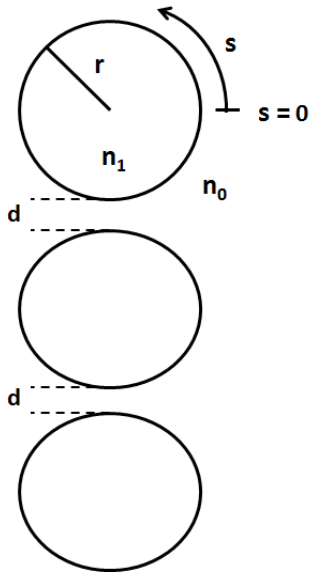

Figure 2.2: A linear array of disks with a distance between the boundary of d. The radius is denoted by r, while the the normalised arc lenght is denoted by s. The refractive indices of the surrounding medium are denoted by n_0 and n_1 referring to the refractive indices of the surrounding medium and the disks, respectively.

According to Snell's law of refraction Eq. 2.1, the direction of the transmitted ray is determined by the refractive indices of the medium for the disk and the incident angle. While the refractive indices are determined by the medium, the incident angle of the ray is directly linked to the momentum, p.

The model used in this thesis is motivated by the model investigated by Ryu and Hentschel [16], who investigated a ray dynamics in a system of coupled disks. In the thesis at hand, the ray dynamics for an infinite array of equally sized disks is investigated. Numerically, the ray dynamics was approached by considering a unit cell consisting of one disk. Each time the ray leaves the unit cell, it was checked if the ray will enter the unit cell again or if it will leave the system.

The program used for the ray dynamics is structured such that the first step consists of translating the incoming parameters p_0 and s_0, respectively into an incident angle and a position on the disk. Because the incoming ray's momentum is defined at the outside of the disks, a ray will never experience internal reflection inside the disk. As the ray transmits into the disk, the ray is refracted according to Snell's law, Eq. 2.1. Hence the angle of the ray inside the disk can never exceed the critical angle for total internal refraction. The script then proceeds to calculate the refraction of the ray according to Snell's law, Eq. 2.1. This angle is used

to find the point where the ray leaves the disk. Finally, the program calculates the angle of the ray leaving the disk to see if it transmits onto the next disk and if so, finds the next coordinates. Finding the values of the new disk is done in the script new_values.m found in the appendix. A single ray will be traced until it leaves the system or the input number of transmits is reached.

The ray trajectories are plotted in different ways. Either as a two dimensional disk system in space as shown in Fig. 2.3 or as a Poincarè surface of section diagram, which is explained in the following subsection. In the disk system, the ray approaches the disk from the top. The script test_plot.m found in the appendix is used to make these plots.

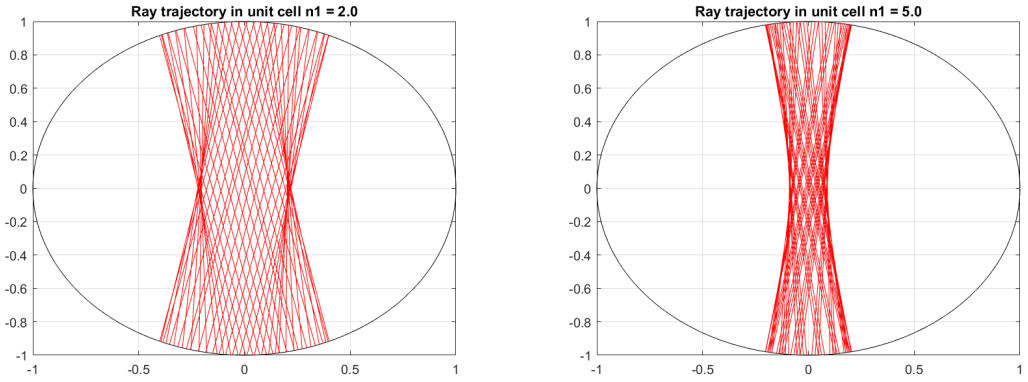

(a) (b)

Figure 2.3: Unit cell: The incident ray approaches the disk from the top. Only the transmitted components are traced and will again approach the unit cell from the top.

2.3 Poincarè surface of section

The idea of Poincaré's surface of section (PSOS) is used to reduce the dimensionality of a dynamical system and to obtain an overview over the dynamics in the classical phase space [3]. The PSOS is established by intersecting the PSOS with the phase space such that intersection consists of a lower number of dimensions than the original. The new created space with a less number of dimensions is called *surface of section*. A well-chosen surface of section provides a good idea of the dynamics of the *phase space*. Phase space is the the space spanned by all allowed values of the variables defining the dynamical system [8]. That is the space of all possible states of the system. The dynamics in phase space shows where the dynamics is

simple and where it is chaotic [3].

The trajectory of a ray in the disk system can be represented by using a PSOS. The trajectory is started by the input parameters. Each time the ray intersects the PSOS, the coordinates of the intersection are stored and plotted in a diagram. This resulting diagram represents the trajectory of the ray in phase space on the defined surface of section. If the ray is traced for a large number of transmissions, a considerable set of points is accumulated:

In system consisting of an array of disks, the surface of section is defined by the variables p and s. The phase space diagram is obtained by plotting the arc length s of the upper half disk, against the momentum p. Each time the ray reaches a new disk, the p and s variables are calculated and stored for the phase space plot.

A typical PSOS diagram is shown in 2.4. The plotted trajectories in this figure consist of rays in stable regimes. A regime is found to be stable if the rays of this regime, stays in the system over a long time. A stable regime can thus contain rays that are periodic and non-periodic.

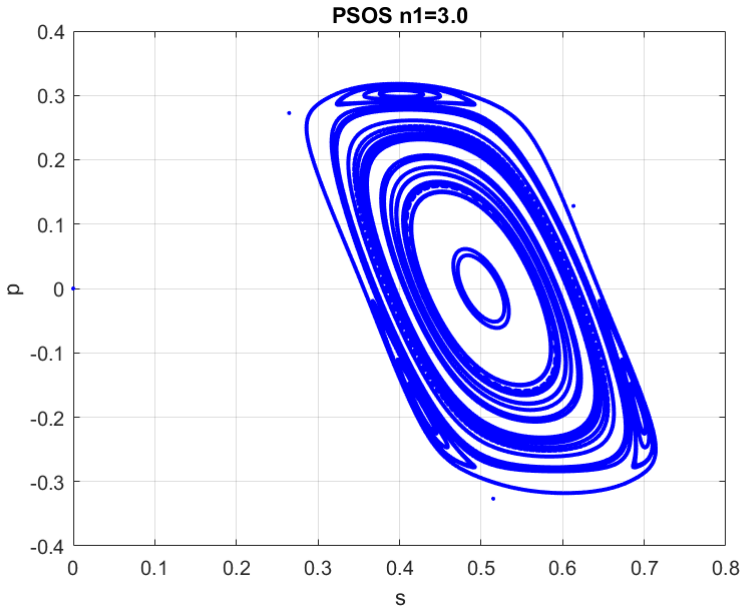

Figure 2.4: A typical PSOS diagram for an array of disk system with $n_1 = 3$ and $d = 0$. 100 rays are plotted with input parameters, s and p set by a random function.

For simulations of many rays, the random function is used. Since the initial random dots created by the random function would fill the PSOS uniformly, they are not plotted. Therefore a parameter called start_plot is defined in the script. This parameter sets a prerequisite for

the ray to transmit through a given number of disks before the coordinates in the PSOS are plotted. By setting a minimum number of disks, start_plot ≥ 1 before simulation, the characteristics of the phase space are getting more visible. This effect is demonstrated in Fig. 2.5. Unstable trajectories are usually leaving the system within a few disks. In Fig. 2.5b unstable trajectories leaving the system are displayed as less dense areas of uniformly distributed points.

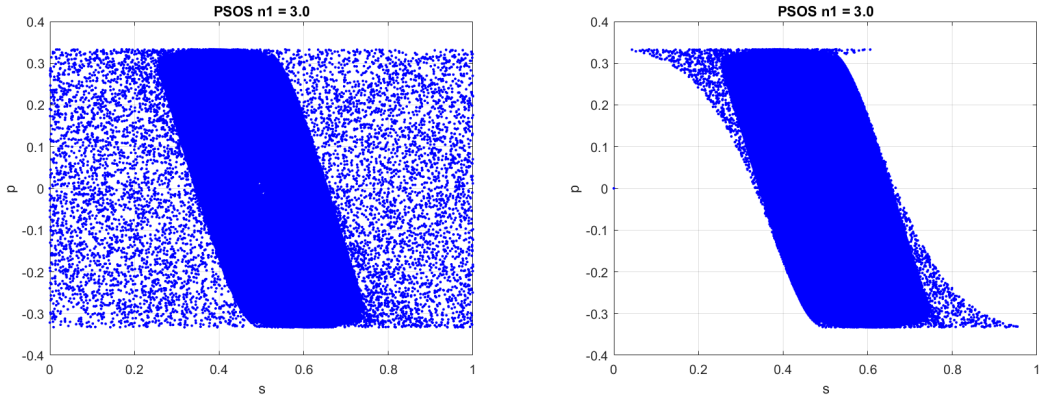

(a) Without use of the start_plot parameter (b) Coordinates from first disk is neglected

Figure 2.5: Diagrams in phase space of 10 000 random rays

2.4 Attractors, fractals, chaos and periodic trajectories

In order to better understand the implication of the plots in phase space, the concepts of attractors, fractals and chaos are briefly introduced in this subsection. These concepts are central in the categorisation of dynamical systems.

The surface of section introduced in the previous section provides a powerful tool for describing the behaviour of chaotic systems. The usefulness of the surface of section lies in its ability to represent behaviour in a geometric form. An example is a pendulum that moves with friction, that eventually comes to a halt. In the phase space this means the trajectory approaches a fixed point. This fixed point is known as an *attractor*, since it attracts nearby trajectories [4]. Roughly speaking, an attractor is what the behaviour of a dynamical system settles down to. An attractor is not necessarily a fixed point: Some system do not come to rest, but instead cycle in a periodic set of positions [4].

Other systems leads to more complex behaviour. Some attractors may not lead to simple cyclic behaviour, but instead to irregular and unpredictable trajectories. For these attractors, the dynamical behaviour of the system cannot always be predicted far into the future. Such motions have been labelled chaotic [13]. Even though it may seem random, chaotic systems are of deterministic evolution [20]. A central characteristic is an exponential sensitivity to the initial condition. This means that small changes in starting position leads to an exponential difference in outcome over time [20].

For each attractor, there are a certain set of points that evolve into that specific attractor. These points are the *basin of the attractor* [1].

Fractals are similar geometric structures that are scale independent. This means that the structure should exist on all scales. For an object, this means that as you magnify a certain area, the same structures should appear. The structures do not necessarily have to be exactly the same, but they must the same type of structure [21].

Attractors that form a fractal structure are *strange attractors* [14]. It is not true that all strange attractors lead to chaotic behaviour, but all chaotic attractors are strange attractors. This makes it evident that the fields of attractors, chaos theory and fractal geometry are connected.

Periodic trajectories are trajectories that cycle between a set of points. This means that for a specific point in the periodic trajectory, the ray eventually returns back to this original point. Examples of such periodic rays are *stationary regimes*. If a ray is started at a stationary regime, the ray will cycle periodically between the exact points of the stationary regime.

3. Ray simulation in array of disk systems

This chapter consists of simulations made in the Matlab scripts found in the appendix. For application in photovoltaics, the structure of nanospheres are closely packed. There is therefore, a larger emphasis on the first section of the closely packed array of disks system. The systems where there is a distance between the disks are briefly discussed in the following section.

3.1 Closely packed array of disks

In the first system, we consider closely packed disks. Closely packed disks are attached to each other forming a continuous array of disks.

3.1.1 Stationary regimes

The stationary regimes are the trajectories of the rays that have an entirely periodic orbit. That is the trajectories that intersects the disks periodically at the exact same points throughout the array of disks. The simplest stationary regime is the ray that travels from the top of the system and in a straight line through all the disks. This stationary regime is shown in Fig. 3.1 and is independent of the refractive indices of the system.

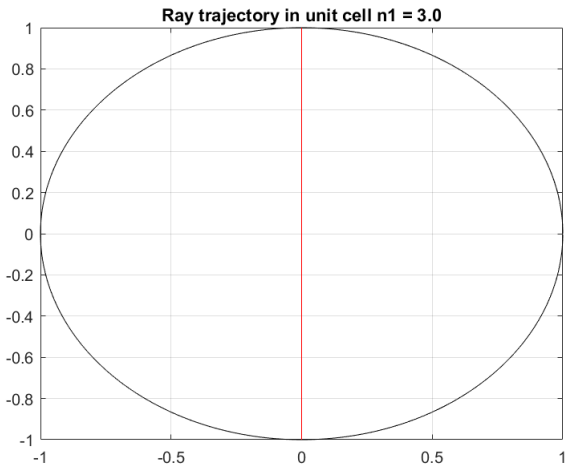

Figure 3.1: The simplest stationary regimes trajectory. The ray is initiated at $s_0 = 0.5, p_0 = 0$ and $n_1 = 3$

Another stationary regime can be found by starting the ray at the top of the disk, $s_0 = 0.5$, and an initial momentum, p_0, determined by Eq. 3.1.

$$p_0 = \frac{n_1}{n_0} \cdot sin(cos^{-1}(\frac{n_1}{2 \cdot n_0})) \tag{3.1}$$

This stationary regime is clearly restricted by the refractive index. In a system of closely packed disks, where $n_0 = 1$, this stable regime disappears, when the refractive index increases beyond $n_1 = 2$, since $cos^{-1}(x)$ does not give a solution for $x > 1$. For a system of refractive index $n_1 = 1.8$ the stationary regime is plotted in Fig. 3.2.

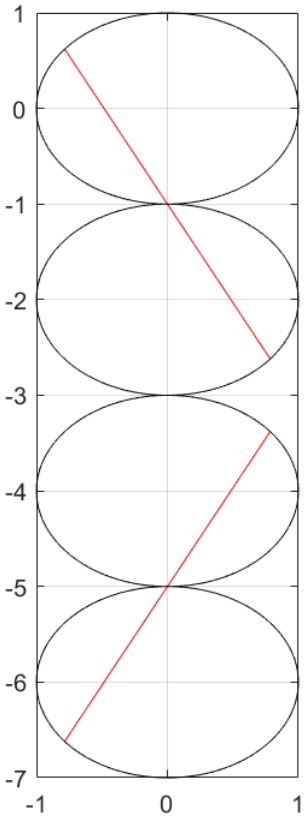

Figure 3.2: A stationary regime for disks of a refractive index, $n_1 = 1.8$. The ray's initial conditions, $s_0 = 0.5$ and p_0 determined according to Eq. 3.1. The ray's trajectory is periodic over with a 4-disk periodicity.

The Poincaré surface of section of this stationary regime is plotted as shown in Fig. 3.3. It clearly consists of four exact points in phase space. For the simplest stationary regime, the PSOS-diagram is not plotted as it simply is a single point, $s = 0.5, p = 0$

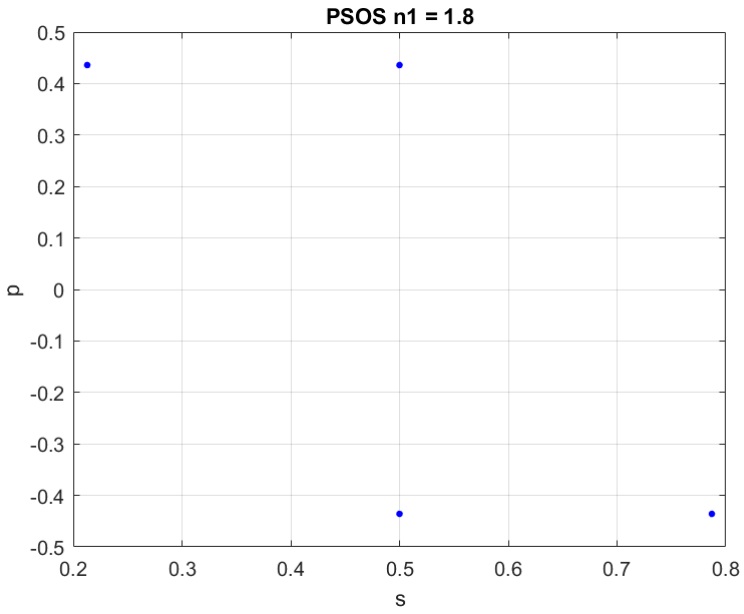

Figure 3.3: The PSOS of the stationary regime shown in Fig. 3.2. The trajectory consists of exactly four points

3.1.2 Reliability of the script

In order to make sure the simulations were reliable, testing of the scripts was performed. To make sure that the ray trajectories are simulated correctly, a test script was made to visualise the rays' trajectories through the disks. This made it possible to quickly check for any obvious mistakes in the program by graphically tracing the ray and its angles of incidence and refraction at the boundaries of the disks when the input values changed. It also demonstrated the continuity of the rays as they transmitted through the disks. Different initial conditions were tested to make sure all parts of the programs are tested. Furthermore, the tracing graphically showed the necessary symmetry of the trajectory in accordance with the symmetry of the disk systems. The test program, test_plot.m is found in the appendix.

Calculations and tracing of rays were also done separately in order to make sure that the output values of the script were accurate.

In order to find the intersection between the ray and the disk, the program solves the system of a linear line and circle. In the special case of the stationary regime, the ray travels in a vertical line between the disks. For the program, this means it has to solve the equation of a line with a gradient approaching infinite. To solve this specific case, a loophole was made

for this case. For sufficiently high gradients, the x-coordinate of the intersection at the new disk is set equal to the x-coordinate of the previous disk.

3.1.3 Phase space

To interpret the behaviour of the accumulated PSOS diagrams of many rays later on in this section and to better understand the behaviour of each single ray as the system and input values changes, rays are first studied individually.

Figure 3.4 shows the phase space trajectory of a single simulated ray with different script parameters. The initial conditions of the ray are chosen arbitrarily to $s_0 = 0.551$ and $p_0 = 0.1$. Initial values close to a centre at $s_0 = 0.5$ and $p_0 = 0$ are chosen simply because these areas are intuitively more stable and thus do not leave the system very quickly. Figure 3.4a shows this ray's trajectory in phase space through 50 disks. Even though the set of points is limited, the elliptic structure is already clear. In Fig. 3.4b the same ray is simulated through 5000 disks. Each time the ray intersects a new disk, a new point is added on this ellipse. This elliptic structure clearly represents a stable regime. The ray's trajectory is trapped in this elliptic structure and both the s- and p-values are restricted by a maximum displacement from the centre at $s = 0.5, p = 0$.

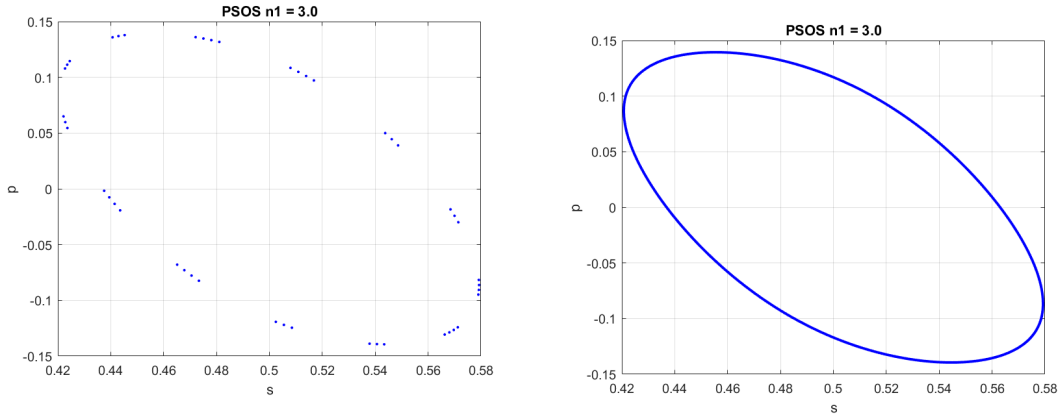

(a) Trajectory in phase space simulated for 50 disks

(b) Same ray traced for 5000 disks

Figure 3.4: Trajectory of the ray with input values $s_0 = 0.551$ and $p_0 = 0.1$. $n_1 = 3$

Apart from the clearly periodic stationary regimes, there are an approximate periodicity for the other stable trajectories in these simulations. Even though the trajectory of these stable

rays never return to its original point, the trajectories periodically cycle between points in the same approximate area in the disk system. This periodicity is demonstrated further in the "Ray trajectory in disks" subsection.

With fixed values of $n_1 = 1.8$ and $s_0 = 0.5$, different input values of p_0 were simulated separately in the interval $0-0.2$ with a differential of 0.01. For values of p_0 over 0.3, the trajectories create more complicated structures and a lower amount of rays stabilise. The most notable result of this, shown in Fig. 3.5, is the maximum radius of the ellipses' dependence on p_0. As the input momentum increase, so does the maximum radius. For diagrams of several rays in phase space, shown in Fig. 3.5d, this is what creates the structure of the accumulated diagrams.

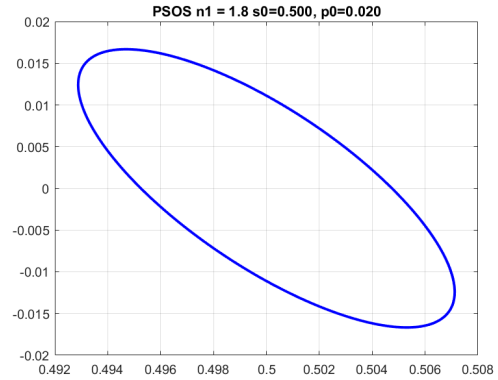

(a) $p_0 = 0.02$

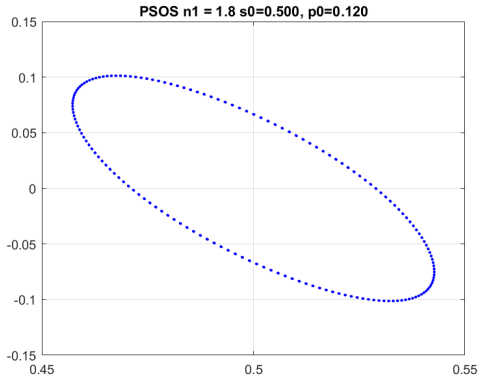

(b) $p_0 = 0.12$

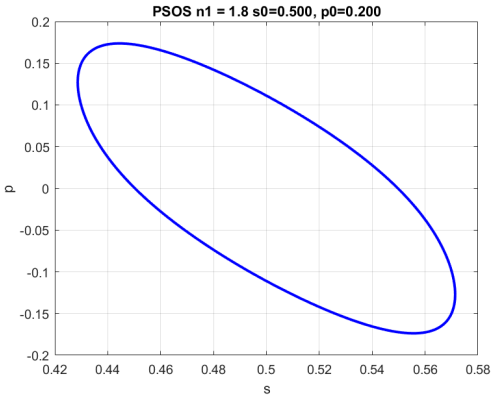

(c) $p_0 = 0.2$

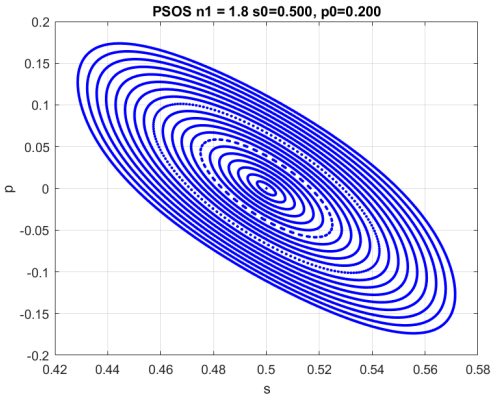

(d) Accumulated plot of rays with p_0 values in the range of 0 - 0.2

Figure 3.5: A look at variable values of p_0 with fixed $s_0 = 0.5$ and $n_1 = 1.8$

In general, as s_0 moves away from the centre and the $|p_0|$-value increase, so does the maximum radius of the ellipse. Intuitively it has the inverse relation to the refractive index as the

rays' momentum inside of the disks reduces by the factor $\frac{1}{n_1}$.

All p_0-values in the range $0-0.3$, lie inside a stable regime forming an elliptic structure. However, as the value increase further, the dynamics completely change. Most of the rays form a seemingly random pattern and they all leave the system within the first 100 disks. As these rays are accumulated, they do however form somewhat of a regular pattern as can be seen in Fig. 3.6d.

When p_0 reaches 0.64 the dynamics dramatically changes again. The rays with p_0-values in the interval $0.64-0.88$ all form four separate structures in the peripheries, with the same centres, but different radius. Similar to the stable trajectories near the centre, these four separate structures form four new stable islands.

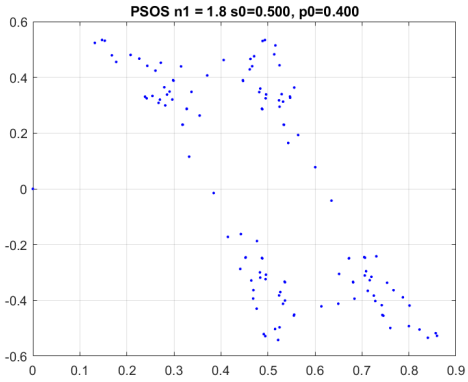

(a) $p_0 = 0.4$

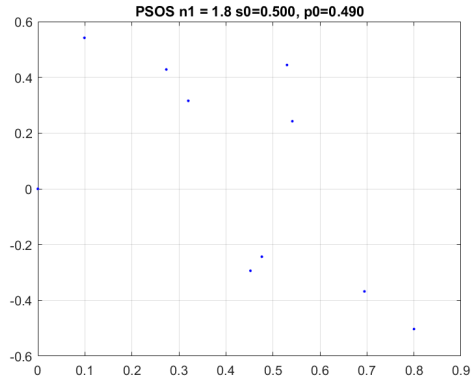

(b) $p_0 = 0.49$

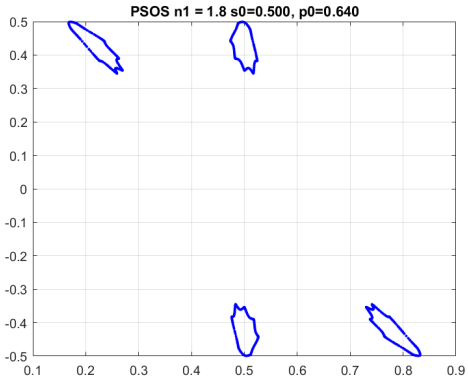

(c) $p_0 = 0.64$

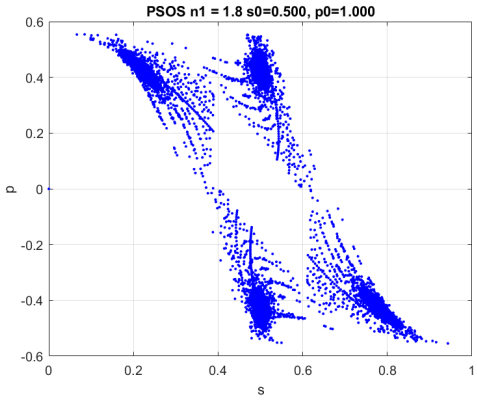

(d) The rays where $s_0 = 0.5$ and p_0 range from 0.3 to 1

Figure 3.6: Variable values of p_0 with fixed $s_0 = 0.5$ and $n_1 = 1.8$

In order to illustrate the dynamics related to these four separate islands, we consider a single ray belonging to these islands.

Figure 3.6c shows the single ray starting at $s_0 = 0.5$, $p_0 = 0.64$. This ray produces four separate, stable islands in the periphery. Furthermore, they are clearly connected as one single ray periodically bounces from one island to the next, alone creating the four structures. A simulation of rays with p-values ranging in the stable interval of 0.64-0.88, is shown in Fig. 3.7. The rays here form closed structures of different sizes. From the stationary regime plot, Fig. 3.3, it is evident that these four islands in fact revolves around the fixed points of the stationary regime. Just as for the central island, which revolves around the simplest stable regime. If the initial conditions of the ray slightly changes from the stationary regime their trajectory periodically revolves around these points. With just a tiny displacement from the stable regime, small closed structures are created, revolving around the points of the stable regime.

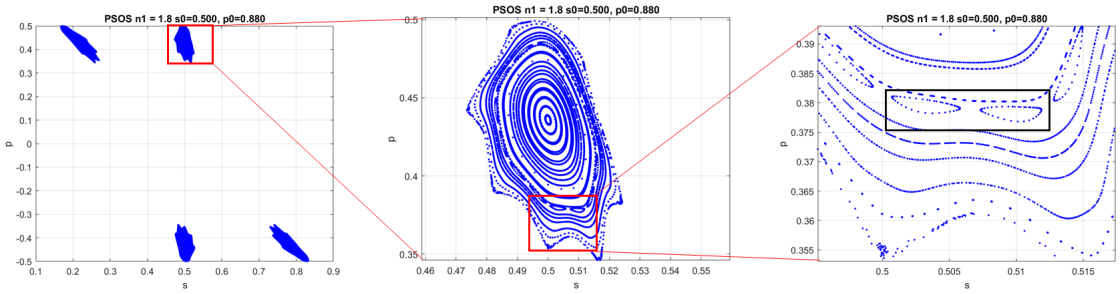

Figure 3.7: A closer look at the rays where $s_0 = 0.5$ and p_0 in the range of $0.64 - 0.88$.

Figure 3.7 shows the accumulated graph of 25 rays with p_0 ranging between $0.64 - 0.88$. Their trajectory create four separate islands in the periphery. As we magnify area of one of the islands further, new closed structures are formed as marked in black in Fig. 3.7. These new ellipses are formed by the single ray where $p_0 = 0.87$.

Examining one of the four islands closer, closed elliptic structures are again found revolving around the centre. By simulating rays from this area, we see that these form an additional set of closed ellipses around different centres with different radii, Fig. 3.8. This may suggest the existence of more complex stationary regimes than previously shown in the stable regime subsection.

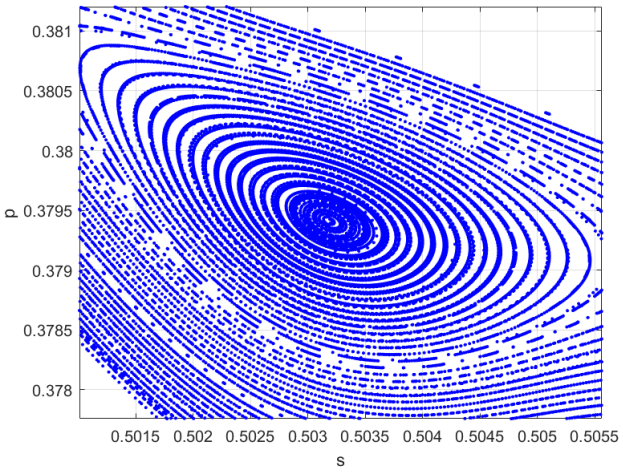

Figure 3.8: A closer look at elliptic structure highlighted in the rightmost part of Fig. 3.7

Figure 3.6d shows a square shaped figure that encloses the separate islands. The rays that create the square shaped figure are not entirely stable. The start_plot parameter determines the number of disks a single ray has to transmit through in order to be plotted. If this parameter is increased, the unstable rays also vanish from the plots. In order to investigate the areas in this system that are actually stable, the start_plot parameter was increased. Figure 3.9 shows the same simulation starting to plot after each ray has transmitted through 1000 disks. This plot shows that there are several fully stable islands for this system.

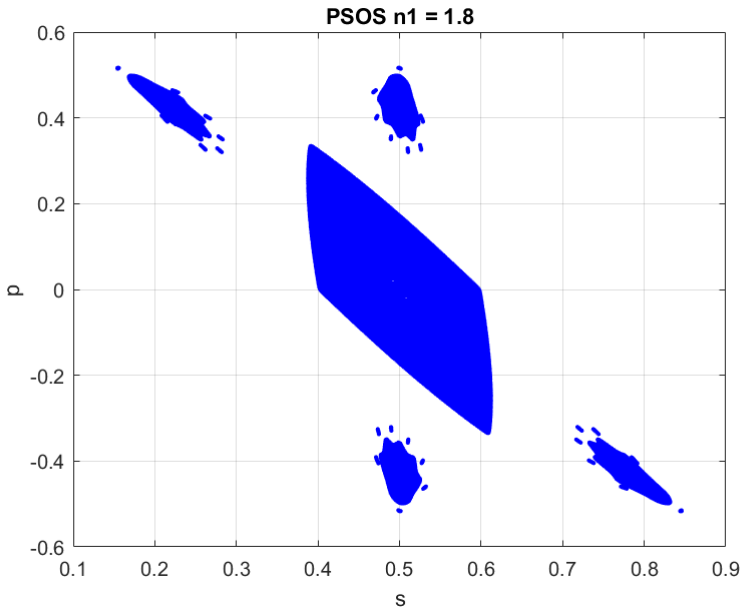

Figure 3.9: n_1 = 1.8, 100 000 random rays and start_plot = 1000

The Fig. 3.9, shows that the fully stable area is actually a lot smaller than the area covered in Fig. 3.6d. Each ray initiated in the stable island areas stabilises into a stable regime. This means that there are an infinite amount of stable regimes within the island and that this entire area are covered with intersections of rays as the number of rays with different initial conditions approach infinite.

As for variable values of p_0, the same procedure as before has been used for a range of input values s_0 with a fixed initial momentum at $p_0 = 0$. Because of symmetry in the disks only values of $s_0 \leq 0.5$ have been considered. As the value approaches the edges of the island, the geometry changes from elliptic to a more square-like structure. However, the structures of the stable regimes do not intersect at any point, making the set of points for each stable regime unique.

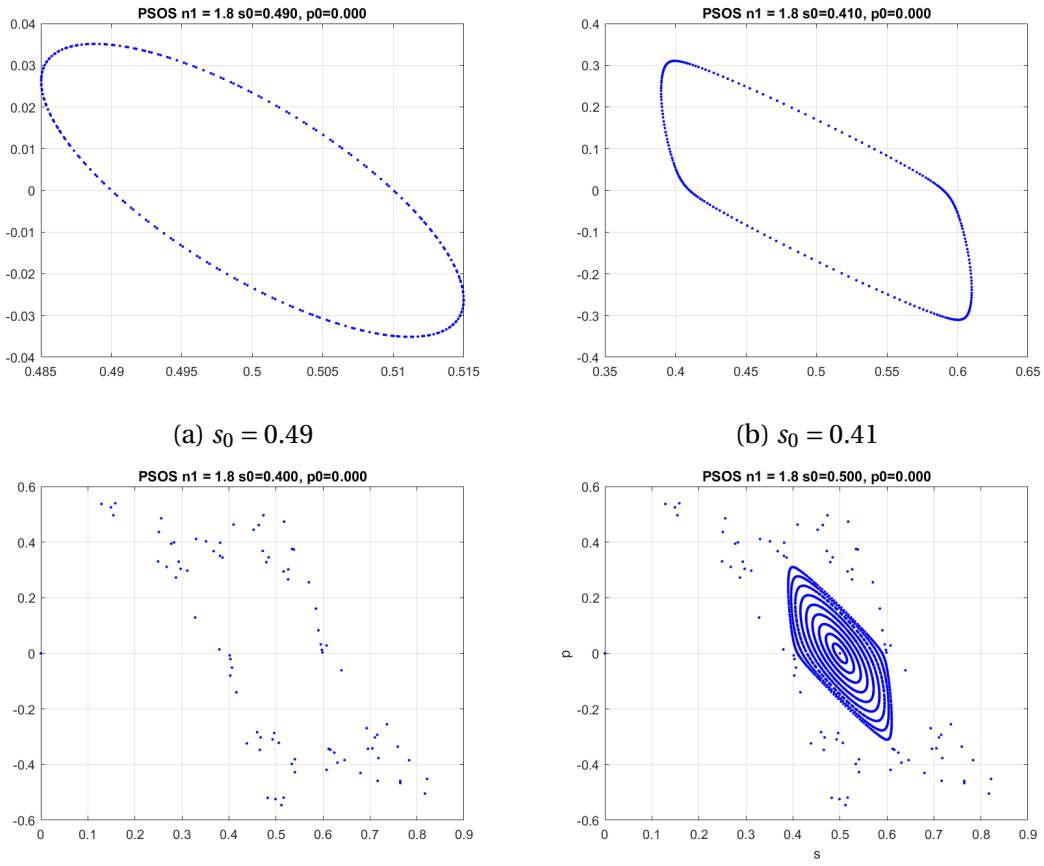

(a) $s_0 = 0.49$

(b) $s_0 = 0.41$

(c) $s_0 = 0.4$

(d) Accumulated plot of rays with s_0 values in the range of 0.2 - 0.5

Figure 3.10: A look at variable values of s_0 with fixed $p_0 = 0$ and $n_1 = 1.8$

The analysis of variable initial values of s_0 and p_0 revealed the shapes of the stable regimes

in the PSOS. The stable regimes form defined areas in the phase space, which have the form of circles or ellipses in the PSOS. Each ray that starts on this circle or ellipse inside the island travels along a circle or ellipse in the PSOS.

All the stable orbits form closed circles or ellipses. For sufficiently long simulations of a single ray, the circles and ellipses form a continuous line in the PSOS. Therefore, for simulations of many rays in phase space, the parameter no_of_transmits, which decides the number of transmits of the ray is increased. If the parameter is low, the structure of each ray become less apparent as demonstrated earlier, Fig. 3.4a. As the number of rays are increased, more geometric structures are created by rays approaching the disk from different positions and angles. The following plots, Fig, 3.11, display six PSOS diagrams simulated by the PSOS.m script for different values of n_1. Each plot is made up by 1000 rays with random initial conditions bounded by $0 \leq s_0 \leq 1$ and $-1 \leq p_0 \leq 1$.

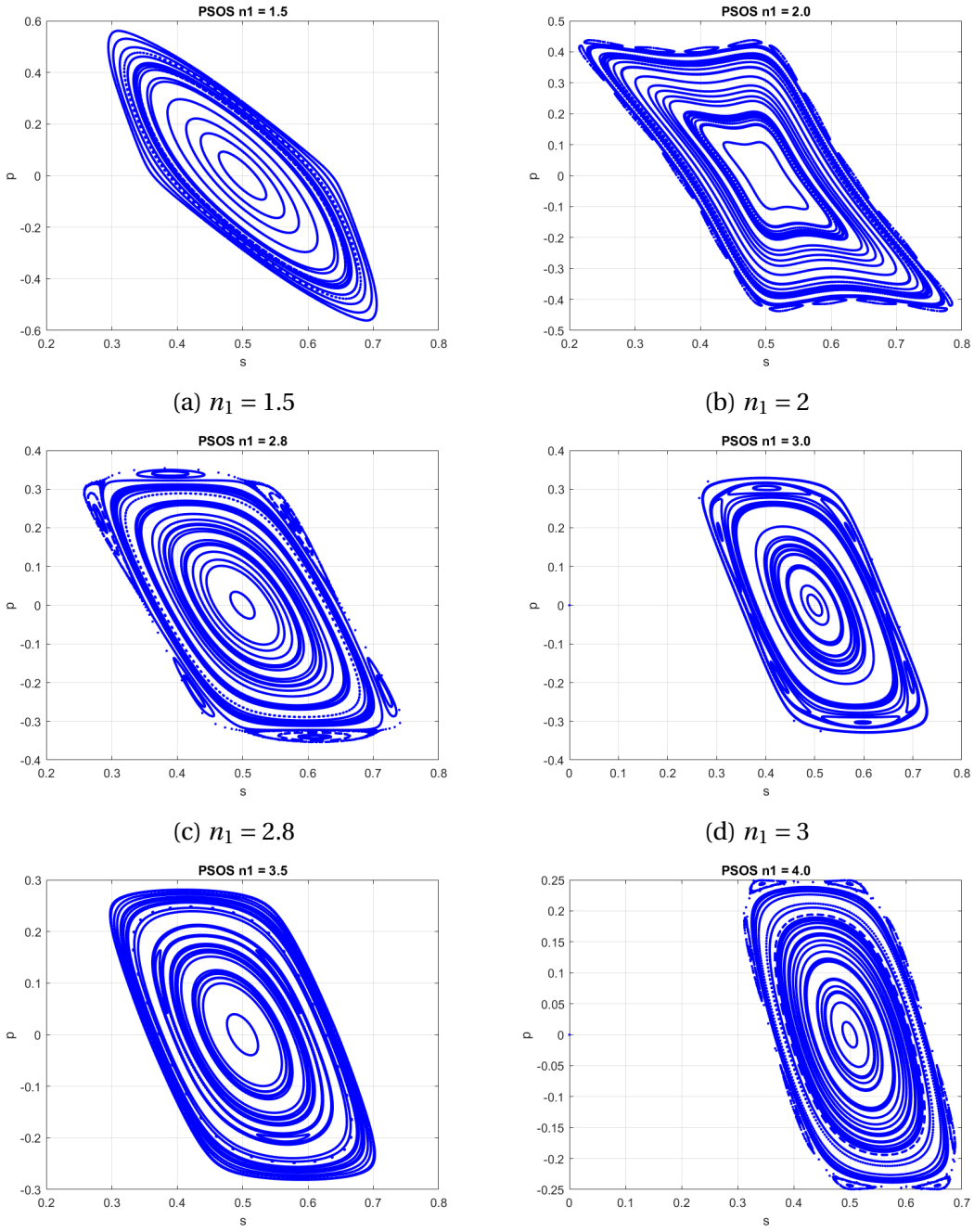

(a) $n_1 = 1.5$ (b) $n_1 = 2$

(c) $n_1 = 2.8$ (d) $n_1 = 3$

(e) $n_1 = 3.5$ (f) $n_1 = 4$

Figure 3.11: Plotted phase space diagrams of 100 random rays with different refractive indices

In Fig. 3.11, the different plots are simulated with different refractive indices. When many random rays are simulated, it is possible to get an idea of the size of the stable island. The island of each plot represent the stable regime for the given system. Rays that had initial conditions outside of the island left the system within the minimum limit of transmissions required by the start_plot parameter of the script. The size of the islands therefore act as a

measurement of the amount of rays trapped in the system. We assume that the area covered by stable islands is connected to the efficiency of solar cells. This assumption is justified, since stable regimes may be related to resonances that exist in the corresponding wave system and resonances can again be directly related to the absorption efficiency of solar cells. However, a comparison of the wave properties with the ray dynamics of the systems investigated in this thesis, is beyond the scope of the thesis.

If we consider the phase space diagram of $n_1 = 4$ in Fig. 3.11f, there is one big stable island covering an area around a centre at $s = 0.5$, $p = 0$. If the initial conditions of the ray are moved out of the stable island, the trajectories in phase space are seemingly random and the ray leaves the system quickly. The reason is because rays enters some sort of downwards spiral. If the values of s and p are outside of the island, they are not part of this downward spiral. The unstable trajectory leads to larger displacements in phase space, which in turn again leads to a further increase in the s- and p-values. If two single rays are started next to each other with a given distance in phase space, this means that as the ray moves in the system, the distance between them will exponentially grow until they both leave the system.Therefore, the array of disk systems in phase space consists of an island of stable trajectories in a sea of chaos.

An unstable ray leaves the system especially quickly for a disk system of a larger refractive index. This is because the rays are more scattered as they exit the disks. According to Snell's law, Eq. 2.1, the angle of the rays exiting the disks are increased proportional to the increase in refractive index.

The values of p plotted in this thesis represent the momentum inside the disk. Thus, the size of the refractive index is related to the largest possible value of p. Due to refraction, the absolute value of p for the transmitted components inside the disks cannot exceed the limit of $\frac{n_0}{n_1}$, where $n_0 = 1$. However, for values of $|p|$ larger than $\frac{n_0}{n_1}$ in phase space, stable regimes of totally reflected orbits exist inside the disk. This means that the area covered by stable regimes is not only determined by the stable regime obtained for values of p below $\frac{n_0}{n_1}$.

For values of $n_1 < 2$, the island stretches out diagonally. This means that the system only stabilise for more specific combinations of p and s. However, when the n_1-value gradually increases, the area of the island also increases. The increased area of the island is due to the fact that the range of accepted $|p|$-values approaches the limit of $\frac{n_1}{n_1}$ as n_1 increases. As

it increases above $n_1 = 2$, the geometry transitions from a squared figure to a more elliptic structure, making it more sensitive to s-values differing from $s = 0.5$. The analysis of finding the optimised refractive index of the disks which gives the largest area, is therefore a compromise between the range of s- and p-values that leads to a stable trajectory.

To increase the accuracy of the size of the islands, a larger number of rays are calculated as shown in Fig. 3.12. As a result, the stable regime within the stable islands is completely filled, while rays outside of the island quickly leaves the system and are therefore not visible. As demonstrated, if a ray is started in a stable regime, it stays in the system with a trajectory forming for example a circle or an ellipse. It is hypothesised, that the total area of the stable regime is directly related to the absorption efficiency of a solar cell by the reasons given above.

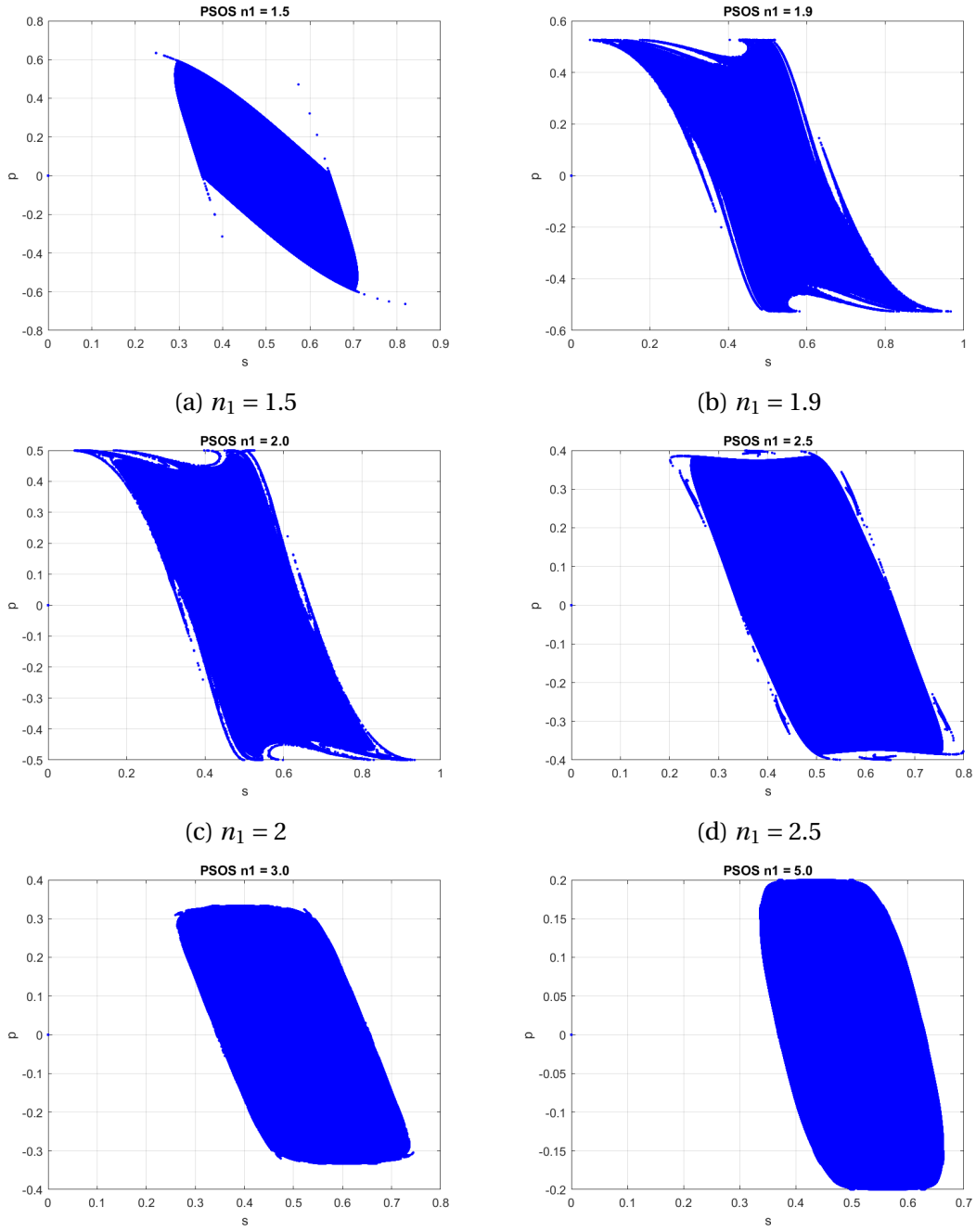

(a) $n_1 = 1.5$ (b) $n_1 = 1.9$

(c) $n_1 = 2$ (d) $n_1 = 2.5$

(e) $n_1 = 3$ (f) $n_1 = 5$

Figure 3.12: Variable values of p_0 with fixed $s_0 = 0.5$ and $n_1 = 1.8$

The area of the islands represent the fraction of rays with varying initial conditions that enter a stable trajectory. Considering the limit of the rays maximum momentum, $|p_{\max}| = \frac{1}{n_1}$, it can be concluded by considering the sizes of the stable regimes in Fig. 3.12, that we expect the refractive index of the disks which leads to the highest absorption efficiency might be in the area of $2 \leq n_1 \leq 3$.

3.1.4 Ray trajectories in disks

This subsection studies the trajectories of different rays inside the disks. The analysis of the rays behaviour inside of the disks may further improve the understanding of the rays behaviour in the array of disks system. Furthermore, identifying the areas with a high density of rays is interesting, as these areas may intensity areas of wave functions in the corresponding wave system. High intensity areas may again refer to an increased absorption efficiency in these areas.

Figure 3.13a shows a ray which is visualized for bounces in 50 disks. The trajectory in the unit disk is clearly restricted in its horizontal motion. The horizontal range of the ray is determined by the refractive index of the disks, as well as the initial conditions which determines the stable regime on which the ray is initiated. In general, as s_0 moves away from the centre and the $|p_0|$-value increases, the horizonal range increases. Intuitively it has the inverse relation to the refractive index as the rays' momentum inside of the disks reduces by the factor $\frac{1}{n_1}$. This relationship is shown by Fig. 3.13c and Fig. 3.13d.

For the disk plots, the horizontal range of motion is also decided by the n_1-values. Larger n_1-values leads, quite intuitively, to a smaller horizontal motion due to Snell's law, Eq. 2.1.

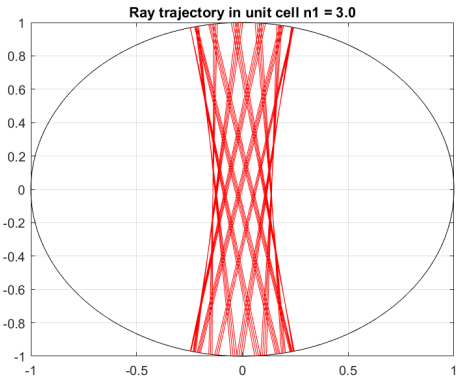

(a) Trajectory in unit disk simulated for 50 disks

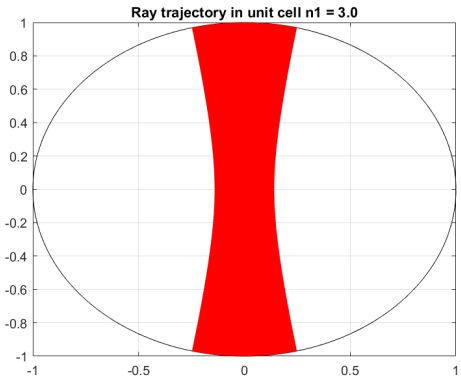

(b) Same ray traced for 5000 disks

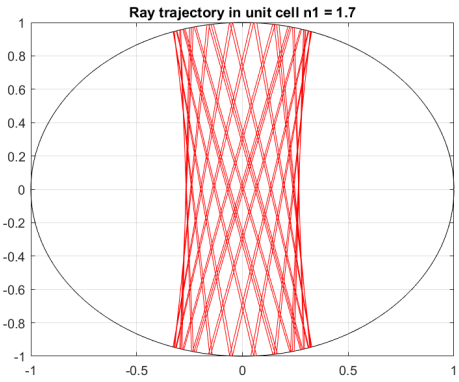

(c) $n_0 = 1.7$

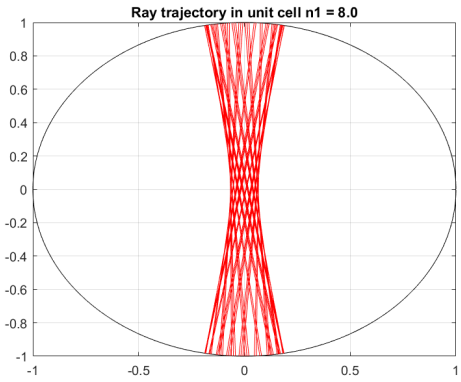

(d) $n_0 = 8$

Figure 3.13: Trajectory of the ray with input values $s_0 = 0.551$ and $p_0 = 0.1$ with refractive index. As n_1 increase, the trajectory in the disks becomes more narrow.

The trajectory in Fig. 3.13a and Fig. 3.13b, corresponds to the Fig. 3.4. It is the same ray in the same system.

The area bound by the maximum horizontal motion range is over time covered with trajectories as both the s- and p-values time vary within the set of points in the stable regime, see Fig. 3.13b.

In Fig. 3.13c and Fig. 3.13d it is demonstrated that the trajectories maximum displacement from the horizontal centre are restricted by the refractive index. Higher refractive index means a more restricted trajectory. This is however, not the only limiting factor for the horizontal displacement of the trajectory in the disk system. For a single ray, the stable regime on which the ray is initiated also has to be considered. Shown in the phase space section, the rays initiated with a displacement from the centre at $s = 0.5, p = 0$ stabilises into a stable

regime with radius dependent on the magnitude of the displacement. Shown in Fig. 3.14, the ray started with a larger $|p|$-value has a larger horizontal range of motion in the disk.

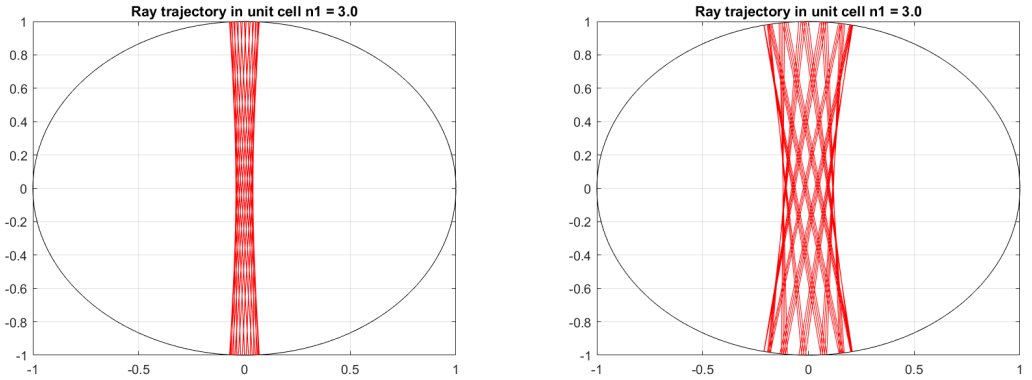

(a) Trajectory of the ray initiated with $s_0 = 0.5$ $p_0 = 0.01$

(b) Trajectory of the ray initiated with $s_0 = 0.5$ $p_0 = 0.1$

Figure 3.14: Two different rays initiated in the same system, but different momentum p_0.

To investigate the behaviour of the rays further, a stable ray was plotted to demonstrate the horizontal motion of the ray's trajectory over time. Such a ray is shown in Fig. 3.15. In this plot, the ray travels through the disks stacked below each other. An approximate periodicity becomes clear in this plot.

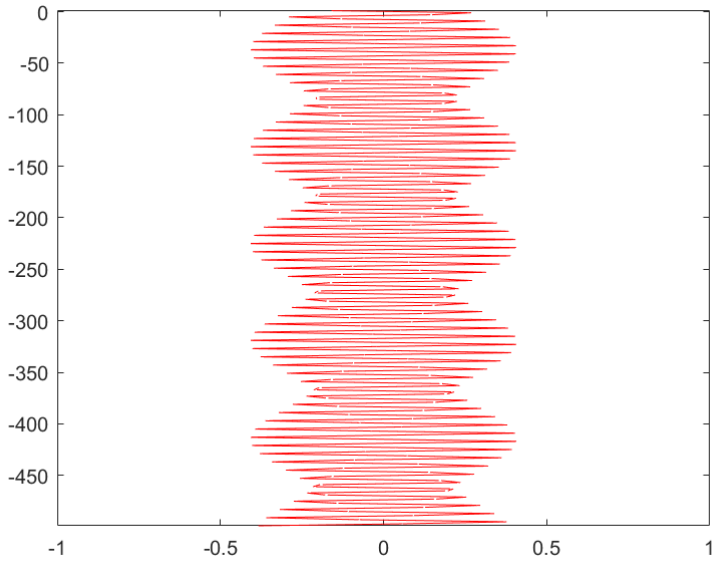

Figure 3.15: The trajectory of the ray $s_0 = 0.551$ and $p_0 = 0.1$ with $n_1 = 2$. The ray starts at the top and moves downwards in the coordinate system. Each disk has a radius of 1.

The periodicity of the ray is also obvious in the graph over $|p|$-values, Fig. 3.16. The period of

the $|p|$-values appear to be in accordance with the s-values shown in Fig. 3.15. However, their relationship is inverted as the minimum values of $|p|$ coincide with the maximum horizontal range of motion of the ray trajectory in Fig. 3.15. That is when the value of s differs from the centre at $s = 0.5$. This is in accordance with the general requirement of an elliptic structure.

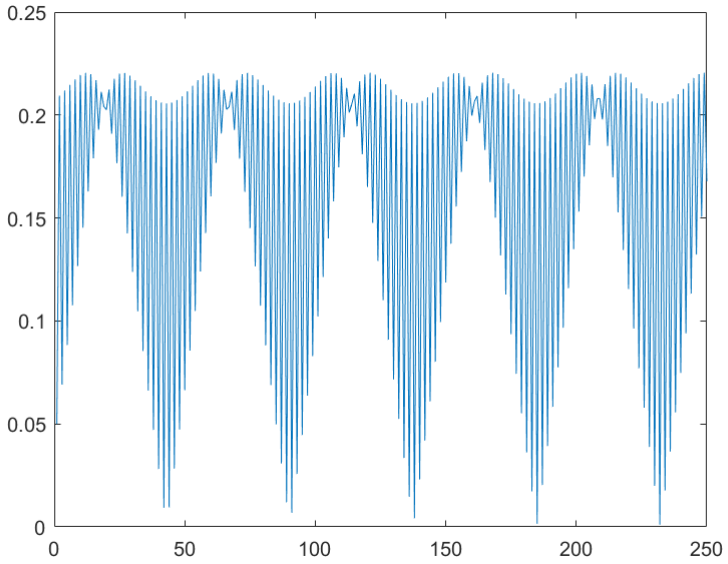

Figure 3.16: The absolute values of the momentum of the ray with start coordinates $s_0 = 0.551$ and $p_0 = 0.1$. $n_1 = 2$

In the previous subsection, it was demonstrated that a ray plotted in proximity of the stationary regime would form an orbit in the PSOS, revolving around the points of the stationary regime. This is confirmed, when observing the ray in the disk system as shown in Fig. 3.17. The figure shows the trajectory of the single ray as it transmits through the array of disks.

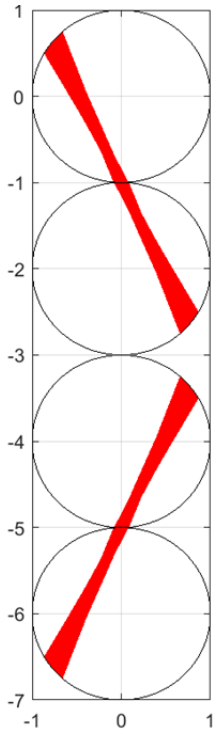

Figure 3.17: $s_0 = 0.5$ and $p_0 = 0.64$

Here the ray is plotted in a 4-disk system as the periodicity of the ray is obvious. The thickness of the trajectory plot is due to rays' displacement from the stationary regime. As shown from in the previous subsection, a stable ray initiated in proximity to the stationary regime, revolve closely around the points of that stationary regime in phase space. If the initial ray is started closer to the stable regime, it periodically revolves around the stable regime with a smaller displacement.

The following figures, Fig. 3.18, shows a magnified area of the same ray as plotted earlier (Fig. 3.13b).

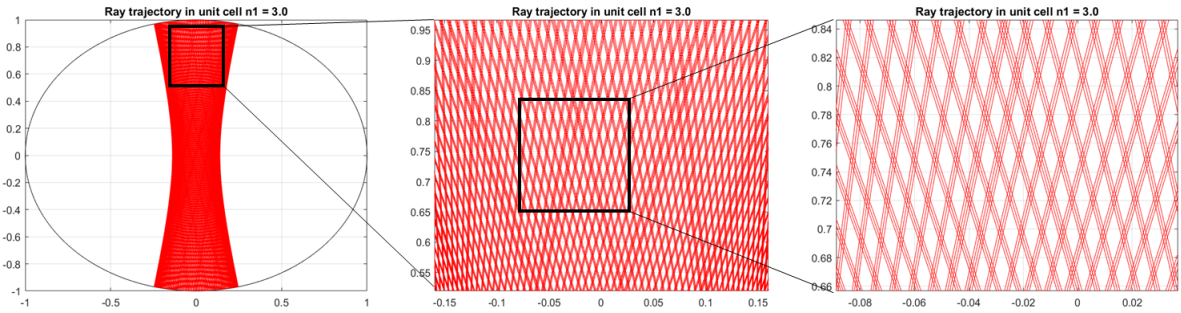

Figure 3.18: Ray simulated with parameters $n_1 = 3$, $p_0 = 0.1$ and $s_0 = 0.551$. Fractal structure is evident as we magnify the trajectory

As the graph is magnified, the rays become less dense as a result of the fact that the number of transmissions has to be limited in the script. However, the geometries are equal on all scales. If the number of transmissions are increased, a smaller area can be zoomed in on and still consist of the exact same structures as shown in Fig. 3.19.

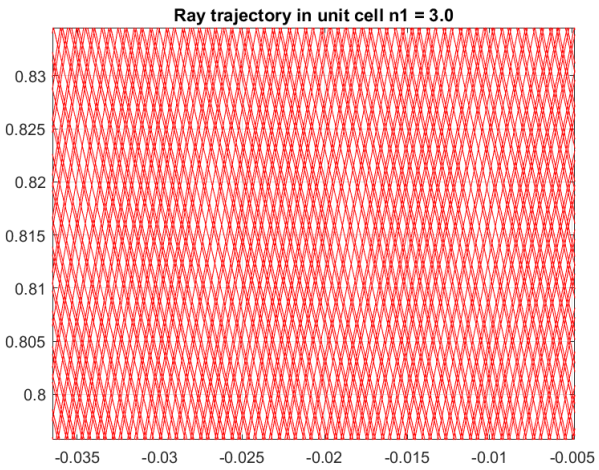

Figure 3.19: A magnified area and the ray simulated with parameters $n_1 = 3, p_0 = 0.1$ and $s_0 = 0.551$, with an increased number of transmission.

3.2 Dynamics in array of disks separated by a distance

This section studies a system where $d > 0$. For nanostructures used in photovoltaics, closely packed spheres are the most relevant. This section will however, briefly discuss a few scenarios where the distance separating the disks, $d > 0$.

The simplest stationary regime, Fig. 3.1, is the same for the systems with distance between the disks and the closely packed array of disks. However, for other stationary regimes, the distance between the disks have to be considered.

Fig. 3.20 shows the phase space plot for increasing values of n_1 in a system where the distance between the disk, $d = 1 = r$. The structures created resemble the islands created in the closely packed system. However, the geometry of the islands in this system looks stretched diagonally. The reason is quite intuitively that the distance between the disks are making the system more sensitive to the position, and momentum moving away from the centre at $s = 0.5, p = 0$. The displacement made by the ray is amplified by the distance between the

disks. Hence, longer distances between the disks make the system more sensitive to these parameters. If the distance separating the disks is increased beyond the radius, the area of the islands quickly decrease until the phase space is entirely unstable.

The analysis of the attached disks system demonstrated that higher refractive indexes of the disks restricted the rays horizontal motion inside of the disks. However, the scattering of the rays exiting the disks is increased proportional with the refractive indices of the disks, n_1 according to Snell's law Eq. 2.1. The horizontal motion of the rays outside of the disks is thus increased with higher refractive indices. Hence, higher refractive indices increase the sensitivity for the p-values and make the islands smaller.

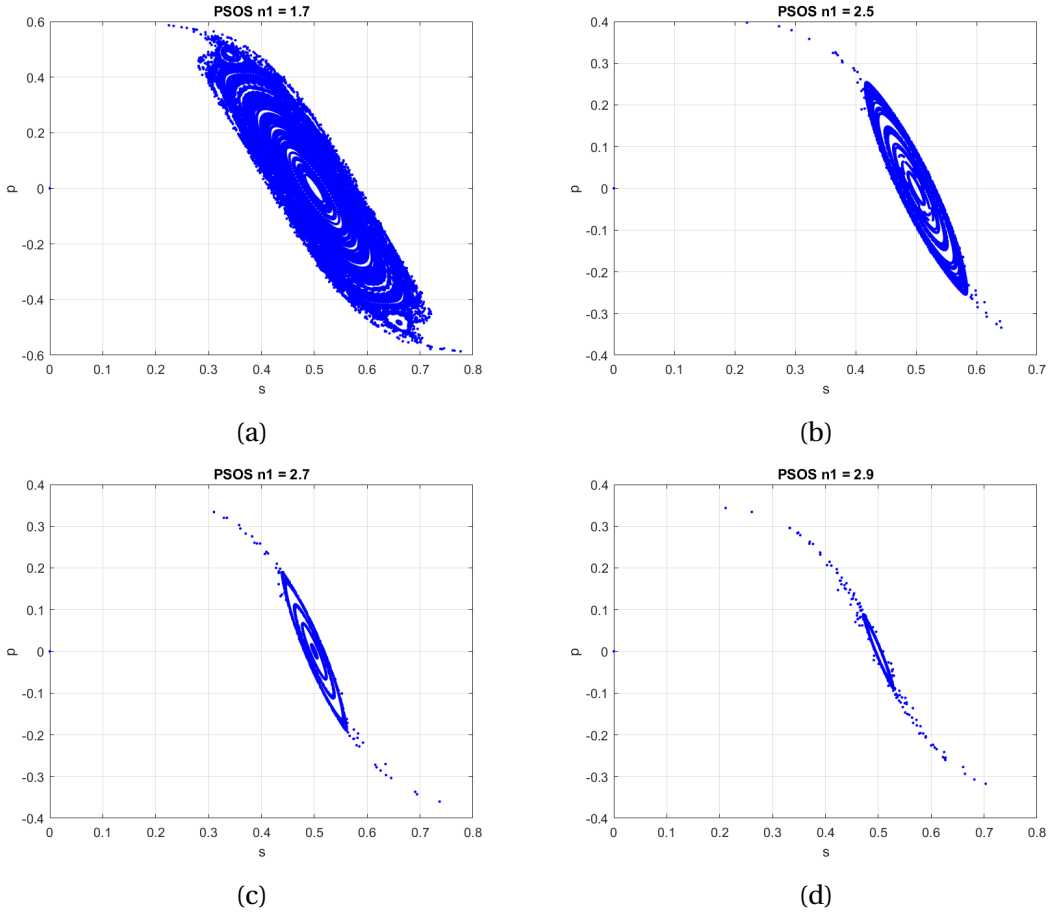

(a) (b) (c) (d)

Figure 3.20: PSOS diagrams of 1000 rays simulated each. $d = 1$, p_0 and s_0 is randomly selected. As the refractive index increase, fewer rays reaches a stable trajectory.

For refractive indices, $n_1 \geq 3$, the stable island completely vanishes when $d = r = 1$

Figure 3.21a, shows the island from the system with a distance between the disks of $d = 1$ when $n_1 = 1.7$. The marked areas are magnified in Fig. 3.21b and Fig. 3.21c. As shown, the

magnified areas display closed structures around different centres in the periphery.

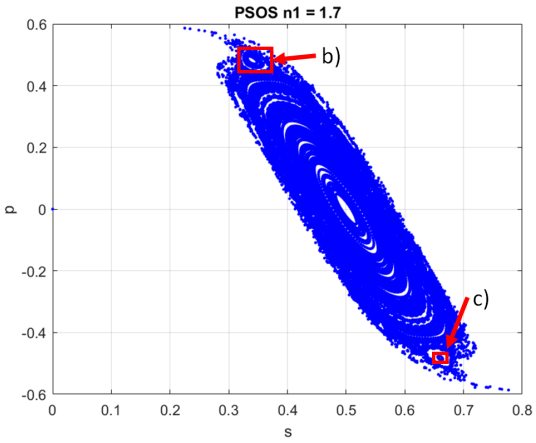

(a) Marked areas indicate the range for subfigures b and c

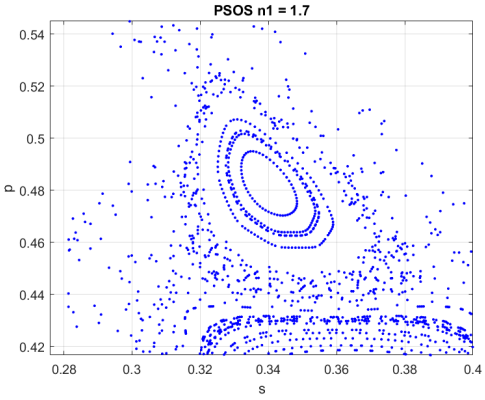

(b)

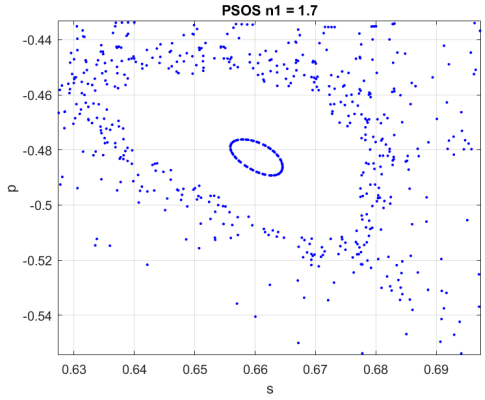

(c)

Figure 3.21: Random rays plotted in the system of $d = 1$ and $n_1 = 1.7$

These structures in the periphery are clearly connected by the rays. By running a simulation in the same system with initial conditions, p_0 and s_0, in the area of the circles shown in Fig. 3.21b, the following Fig. 3.22 was obtained.

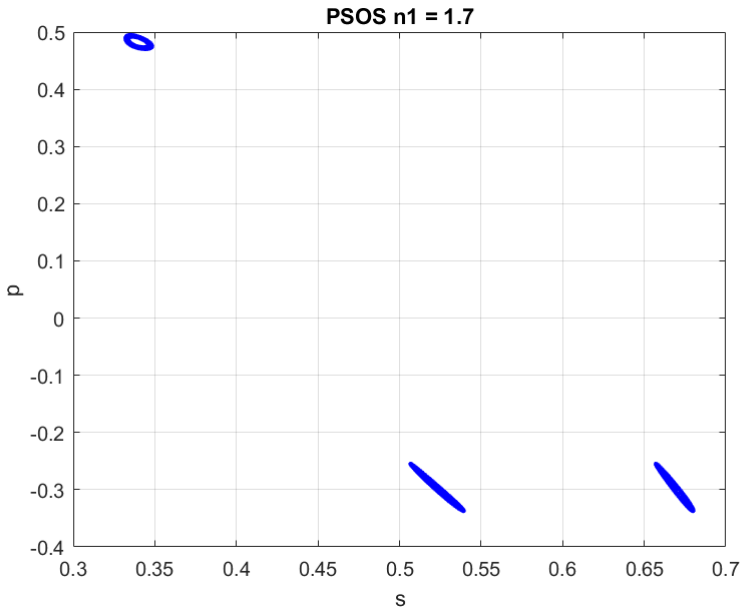

Figure 3.22: Rays simulated with input parameters in proximity of $s_0 = 0.34$ and $p_0 = 0.48$, which corresponds to the structures showed in Fig. 3.21.

In the section of closely packed disks, it is shown that as the initial conditions are differing slightly from the point of a stationary regime, the ray makes closed orbits revolving around the fixed points of the stationary regime. Figure 3.22 shows that for $d = 1$ and $n_1 = 1.7$ there are three islands created by one single ray in the periphery opposed to four as it was for the closely packed system with closely packed disks shown in Fig. 3.6c. This indicates that there is a three-disk periodic stationary regimes in this system.

In the same way as for closely packed disks, the patterns created by the fully stable rays are plotted by increasing the start_plot parameter as a requirement for the ray to transmit through a high number of disks before plotted. The rays that do not enter a stable trajectory are then never plotted. Such a plot is shown in Fig. 3.23.

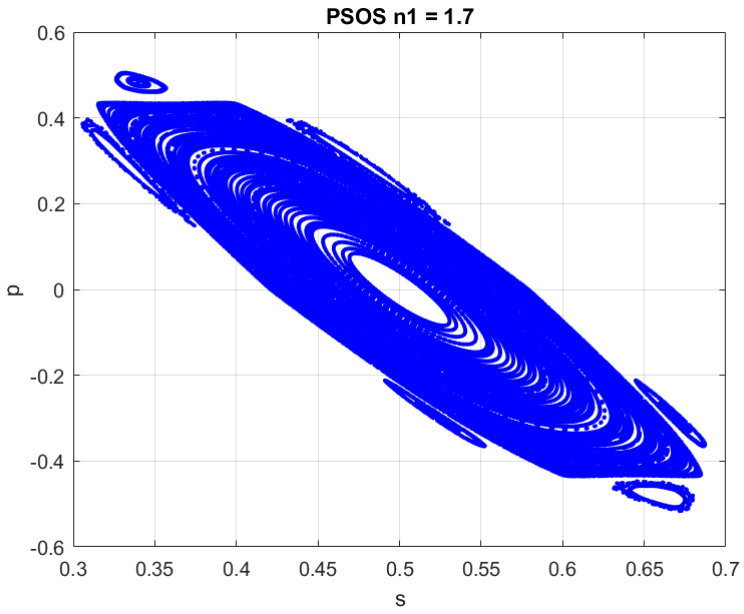

Figure 3.23: Rays simulated in the system, $d = 1, n_1 = 1.7$

Outside of the stable island revolving around the centre, $s = 0.5, p = 0$, there are a total of six separate islands. In the same way as three of these islands are already shown to be connected by the same rays, so are the remaining three. Figure 3.24 is a plot of a number of rays plotted specifically in one of the islands. As shown in the highlighted area, the rays all form orbits revolving around three fixed points.

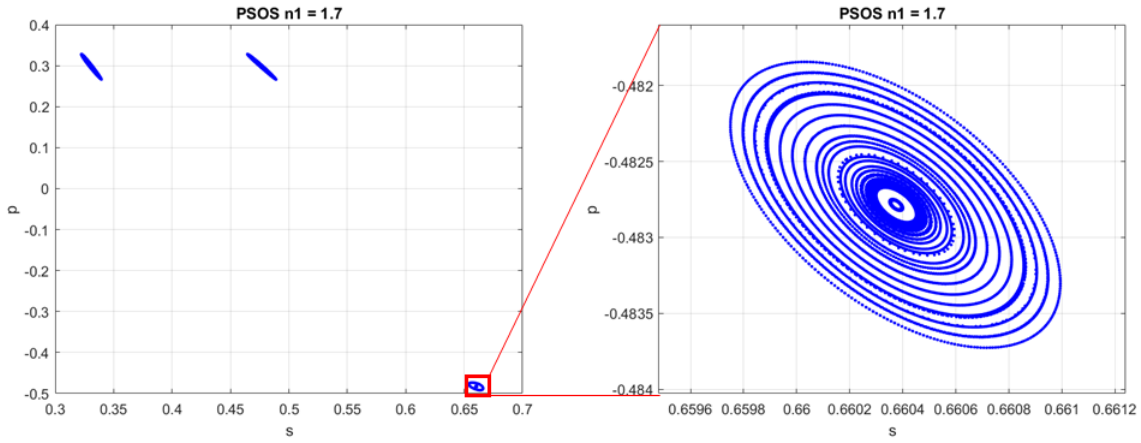

Figure 3.24: Rays plotted with fixed a $s_0 = 0.6603$ and p_0 in the range from -0.8219 to -0.8202. System parameters, $d = 1$ and $n_1 = 1.7$

When a larger amount of rays are simulated, new structures are revealed in the PSOS. Figure 3.25 displays a magnified look at some of the new structures in the periphery. The figure

shows that some rays form new closed structures. This may suggest additional, more complex stationary regimes.

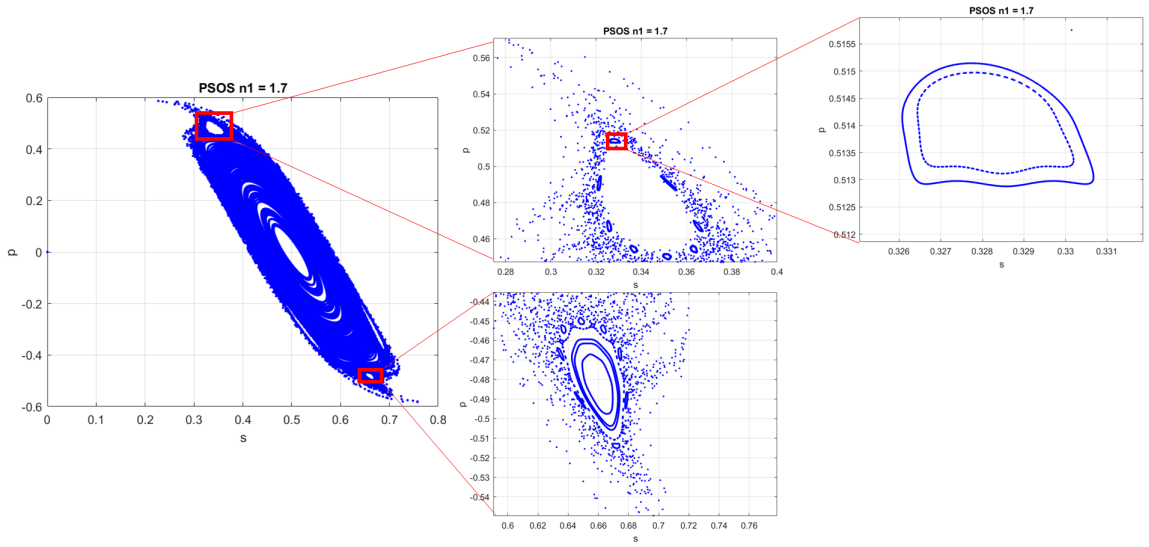

Figure 3.25: A larger amount of random rays plotted in the system, $d = 1$ and $n_1 = 1.7$. The magnified areas show new closed structures formed.

Figure 3.26 shows three plots for different values of d, the distance between the disk boundaries. A high number of random rays was started and the start_plot parameter is set to 1000 disks. Thus, is is expected that all unstable rays have left the system and the rays remaining in the system are stable. Interestingly, the area of the island increases significantly when there is a small distance between the disks.

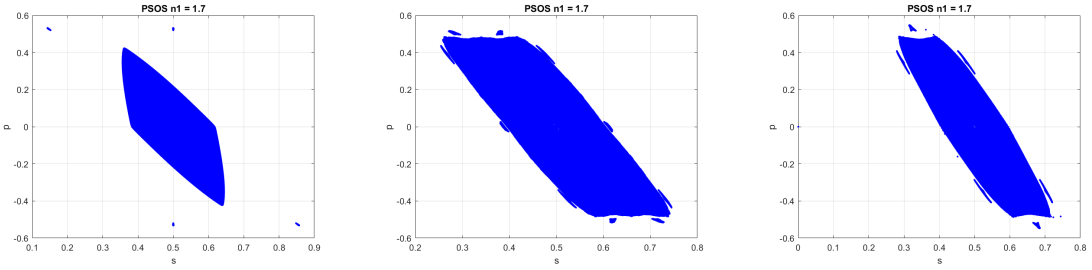

(a) $d = 0$ (b) $d = 0.5$ (c) $d = 0.8$

Figure 3.26: Random rays plotted in the system of $n_1 = 1.7$ and different values of d.

As Fig. 3.26 shows, a small distance between the disks actually makes a contribution to stabilise rays for low refractive indices. For $n_1 = 1.7$, the largest island appear when the distance separating the disks is in proximity of $d = \frac{r}{2}$. However, for refractive indices, $n_1 \geq 2$, the area of the island reduces with increased distance separating the disks. Hence, also reduces

the fraction of rays reaching stable trajectories. This is shown in Fig. 3.27. Larger refractive indices means a larger reduction.

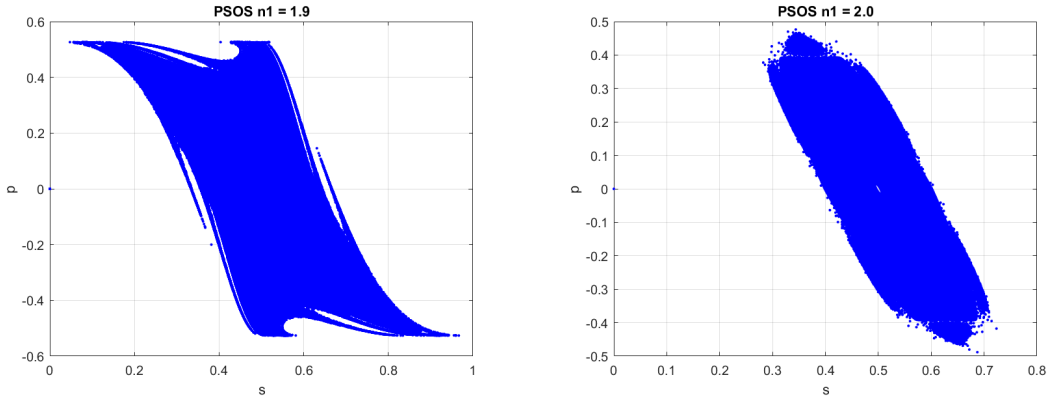

(a) $d = 0$ (b) $d = 0.5$

Figure 3.27: Stable islands in the system, $n_1 = 2$

By this brief analysis, it is clear that generally the islands created in phase space are reduced as the distance separating the disks increases. However, for refractive indices below $n_1 < 2$, a small distance, $d \leq r$, separating the disks can lead to a larger stable area in phase space.

4. Discussion, Conclusions and Outlook

4.1 Discussion

In solar cell applications, spherical nanoimprints are used for increasing the efficiency of the solar cells. The solar cells may be either placed on top of the energy converting material [7], they may be inside the energy converting material [18] or nanospheres may in future be made of energy converting materials. The system investigated in this thesis is simplified. Two major simplifications are made: the spheres are reduced into a two dimensional system of disks and only one array of disks is considered. Therefore, for example rays crossing from one array to another array are not considered. Thus, many rays unstable in the array of disks, could stay in the system by crossing to neighbour arrays, when many arrays of rays are considered. If these effects are to be considered, new stable islands can be expected to form in phase space, but by rays that switch between different array of disks or even travel diagonally. For the trajectories in the unit disk, new stable trajectories would be formed in other directions and possibly alter the distribution of trajectories in the unit disk. However, only the the rays that are stable in one array of disks are considered in this thesis.

Further simplification is made through limiting the ray trajectories to only consider the transmitted components of the simulated rays. Even though the transmitted components of the ray cannot exceed the limit of $|p| > \frac{n_0}{n_1}$ inside the disks, this area in phase space is not empty in systems considering reflected components. Though, they are not considered in the simulations of this thesis, stable regimes of totally reflected orbits occupy this area. An alternative approach could be to implement a selection rule to determine which of the transmitted or reflected component to be traced. Such systems are previously analysed in literature [16]. In this report a selection rule is defined to determine whether the reflected or transmitted

component are traced in a system of coupled disks. The result of this was that for $|p|$-values higher than a critical value for total internal reflection, p_c, straight lines were formed. These represented rays stable whispering gallery modes, trapped in one single disk. The selection rule also lead all initiated rays with $|p| < p_c$ to form an attractor of stationary regime after a phase of transient behaviour.

The ray model is a simplified model that does not consider effects that normally would arise in a system like this. For a more thorough analysis of this system, where the nanospheres' size is in the magnitude of the lights wavelength, the classical ray dynamics evaluated in this system could be compared with Mie resonances and other resonances in the system obtained by wave theory. The ray dynamics could therefore be correlated to the wave dynamics in the system. However, as a simplified model, the ray model makes it possible to make a simulation of the light rays trajectories in a system over a longer period of time. Furthermore, the rays' stable regimes may be correlated with the resonances in the wave system.

4.2 Conclusions

It has been shown that the efficiency of thin-film solar cells can be increased when structuring them with nanospheres [7]. To better understand the reason for this increase, both the wave mechanics and the ray mechanics structures with nanospheres need to be investigated. The frame of this thesis was to explore ray dynamics in a two-dimensional array of disks as a simplified model system for the ray dynamics in thin-film solar cells with nanospheres. It is expected that a better understanding of the ray dynamics in an array of disks will, in future, contribute to understand the absorption of light in solar cells with nanospherical imprints better.

The transmitted components of rays were traced in an array of disks system. A consequence of only tracing the transmitted components is that some rays leave the system quickly. However, for stable rays that stay in the array of disks system, there was no restriction on the length of the array. The analysis of the trajectory of individual rays demonstrated that stable rays form closed elliptic structures in phase space. These structures enclosed the fixed points of the periodic stationary regimes. For plots of accumulated rays with varying initial

conditions, these orbits formed islands of stable trajectories in phase space. These islands represent the fraction of rays that turn into stable trajectories in the system as the rays' initial conditions vary. The surrounding area leads to chaotic behaviour of rays that quickly leave the system.

The simulations of rays in this system were divided into two categories; closely packed disks and disks separated by a distance. The area of the islands were dependent on the refractive index of the disks. For closely packed disks, the area of the island reached a maximum area for a refractive index, n_1 in the the range $2 \leq n_1 \leq 3$. For refractive indices below $n_1 = 2$, it was demonstrated that a small distance between the disks improved the trapping of the rays. However, for larger refractive indices the area of the islands reduced and, in some cases, vanished completely.

4.3 Outlook

This thesis is limited to the effects of rays travelling in an array of disks. In solar cell applications, nanospheres are a covering layer on top of the solar cell, thus containing a large number of parallel arrays of disks. Therefore, it would in future be highly relevant to analyse the cross effects that arise when rays leave one array to enter the adjacent arrays.

To obtain a more adequate understanding of the behaviour of the light in the disk system, the contribution of the reflected light should also be considered. In general, the areas with a high density of rays could indicate big resonances of the plane waves. These areas may change when the reflected components of the rays are considered.

In order to verify that the high resonance areas in the system correspond with the islands in phase space, simulation of waves should be made in the disk system. Simulating waves surrounding the disks should also be considered, as resonances might be found in these areas too.

Bibliography

[1] Abrahams, R. H. and Shaw, C. D. (2016). *Dynamics: The Geometry of Behavior*. Monkfish Book Publishing Company, New York, USA.

[2] Berry, M. V. (1981). Regularity and chaos in classical mechanics, illustrated by three deformations of a circular 'billiard'. *European Journal of Physics*, 2:91 – 102.

[3] Blümel, R. and Reinhardt, W. P. (1997). *Chaos in Atomic Physics*. Cambridge University Press, Cambridge, UK.

[4] Crutchfield, J. P., Farmer, J. D., Packard, N. H., and Shaw, R. S. (1986). Chaos. *American Scientific*, 254:46 – 57.

[5] Grandidier, J., Callahan, D. M., and Munday, J. N. (2012a). Gallium arsenide solar cell absorption enhancement using whispering gallery modes of dielectric nanospheres. *IEEE Journal of Photovoltaics*, 2:123 – 128.

[6] Grandidier, J., Callahan, D. M., Munday, J. N., and Atwater, H. A. (2011). Light absorption enhancement in thin-film solar cells using whispering gallery modes in dielectric nanospheres. *Advanced Materials*, 23:1272 – +.

[7] Grandidier, J., Weitekamp, R. A., Deceglie, M. G., Callahan, D. M., Battaglia, C., Bukowsky, C. R., Ballif, C., Grubbs, R. H., and Atwater, H. A. (2012b). Solar cell efficiency enhancement via light trapping in printable resonant dielectric nanosphere arrays. *Physica Status Solidi A-Applications and Materials Science*, 210:255 – 260.

[8] Gros, C. (2013). *Complex and Adaptive Dynamical Systems*. Springer verlag, Heidelberg.

[9] Honsberg, C. and Bowden, S. Light trapping. `http://pveducation.org/pvcdrom/5-design-of-silicon-cells/light-trapping`. Accessed: 2017-03-06.

[10] IEA (2015). Iea energy technology perspectives 2015. Technical report, International Energy Agency.

[11] IEA-PVPS (2016). Trends 2016 in photovoltaic applications. Technical report, International Energy Agency.

[12] Kelzenberg, M. D., Boettcher, S. W., Petykiewicz, J. A., Turner-Evans, D. B., Putnam, M. C., Warren, E. L., Spurgeon, J. M., Briggs, R. M., Lewis, N. S., and Atwater, H. A. (2010). Enhanced absorption and carrier collection in si wire arrays for photovoltaic applications. *Nature Materials*, 9:239 – 244.

[13] Moon, F. C. (2004). *Chaotic and Fractal Dynamics*. Wiley-VCH Verlag, Weinheim, Germany.

[14] Ott, E. (1993). *Chaos in dynamical systems*. Cambridge University Press, Cambridge, UK.

[15] REN21 (2016). Renewables 2016 global status report. Technical report, REN21.

[16] Ryu, J. and Hentschel, M. (2010). Ray model and ray-wave correspondence in coupled optical microdisks. *Physical Review A, (3)*, 82:1 – 8.

[17] Shah, A. V., Schade, H., Vanecek, M., Meier, J., Vallat-Sauvain, E., Wyrsch, N., Kroll, U., Droz, C., and Bailat, J. (2004). Thin-film silicon solar cell technology. *Progress in Photovoltaics: Research and Applications*, 12:113 – 142.

[18] Shang, A., Qun, L., Zhan, Y., and Zhang, C. (2016). Broadband and wide-angle light harvesting by ultra-thin solar cells with partially embedded dielectric spheres. *Optics letters*, 41:1329 – 1332.

[19] Tipler, P. A. and Mosca, G. (2008). *Physics for scientists and engineers*. W.H. Freeman and Company, New York, USA.

[20] Weisstein, E. W. Chaos. From MathWorld—A Wolfram Web Resource. `http://mathworld.wolfram.com/Chaos.html`. Accessed: 2017-04-25.

[21] Weisstein, E. W. Fractal. From MathWorld—A Wolfram Web Resource. `http://mathworld.wolfram.com/Fractal.html`. Accessed: 2017-04-27.

[22] Zhu, J., Hsu, C. M., Yu, Z., Fan, S., and Cui, Y. (2010). Nanodome solar cells with efficient light management and self-cleaning. *Nano Letters*, 10:1979–1984.

A. Appendix

A.1 PSOS.m

```
%% Plotting PSOS diagram of rays trajectories
%
% This script plots the PSOS diagram for trajectories of a specified
    number
% of rays

%% Input values

s0 = 0.168;
p0 = -0.482785*1.1;

no_of_simulations = 10000; % Number of simulated rays

n0 = 1;                  % Refractive index of the surrounding medium
n1 = 1.1;                  % Refractive index of the disk

r = 1;                   % Radius of the disk
d = 0;

no_of_points = 6000;      % Amount of calculated transmissions per ray

start_plot = 1000;        % Amount of disks passed before it starts
```

```
    plotting

%% Plot

p_array = zeros(no_of_simulations, no_of_points/2);
s_array = zeros(no_of_simulations, no_of_points/2);

rng('shuffle')
for i = 1:no_of_simulations
    s0 = rand;
    p0 = rand*2 - 1;
    [z, s, p] = disk(s0,p0,n0,n1,no_of_points,r,d);
    for j = 1:length(s)
        s_array(i,j) = s(j);
        p_array(i,j) = p(j);
    end
end
for i = 1:no_of_simulations
    length_vector = length(s_array(i,:));
    if s_array(i,start_plot*2) ~= 0
        s = s_array(i,start_plot*2:length(s_array(i,:)));
        p = p_array(i,start_plot*2:length(s_array(i,:)));
        plot(s, p, 'b.')
        hold on
        grid on
    end
end

title(sprintf('PSOS n1 = %.1f', n1))
xlabel('s');
ylabel('p');
```

A.2 plot_ray.m

```
%% Plotting of trajectory in unit disk
%
% This script plots a single rays trajectory in the unit disk. The ray
% approach the unit disk from the top initially and each time it is
% transmitted onto a new disk.

%% Input values

s0 = 0.5;                  % Start position
p0 = 1.8*sin(acos(1.8/2)); % start momentum


no_of_points = 100;        % number of calculated points

n0 = 1.0;                  % surrounding refractive index
n1 = 1.8;                  % refractive index of disk

r = 1.0;                   % radius of disk
d = 0;                     % distance separating the disks

%% Plotting the unit disk

unit_circle = 0:0.01:2*pi;

disk_x = r*cos(unit_circle); % x-coordinates for the disk
disk_y = r*sin(unit_circle); % y-coordinates for the disk

for i = 1:length(unit_circle)
    plot(disk_x,disk_y,'k');
    %axis
```

```
31      grid on
32      hold on
33  end
34
35  %% Plotting the ray
36
37  [z, s, p] = disk(s0,p0,n0,n1,no_of_points,r, d);
38
39
40  for n = 2:2:length(z)
41
42      plot ([real(z(n-1)) real(z(n))], [imag(z(n-1)) imag(z(n))], 'r');
43  end
44  title(sprintf('Ray trajectory in unit cell n1 = %.1f', n1))
```

A.3 disk.m

```
%% Calculates trajectories of a ray inside the disks
%
% Breaks the loop as soon as the ray leaves the system. That is
%
function [z,s_list,p_list] = disk(s0,p0,n0,n1,no_of_points,r, d)

z = zeros(1,no_of_points);
s_list = zeros(1,no_of_points/2);
p_list = zeros(1,no_of_points/2);

for n = 1:no_of_points
    if n == 1
        % first point
        if p0 < 0
            dir = -1;           % Angles are counterclockwise
        else
            dir = 1;            % Angles are clockwise
        end
        phi = s0*r*pi;          % The polar angle
        z(n) = r*exp(1i*phi);   % First point
        theta0 = abs(asin(p0)); % Incident angle
        s_new = s0;

    elseif mod(n,2) == 0
        % Calculating the lower half coordinates in disk
        theta1 = asin(sin(theta0)*n0/n1);% Angle inside disk
        p_new = sin(theta1)*dir;
        delta_phi = pi - 2*theta1;      % Change in polar angle
        z(n) = r*exp(1i*(phi - (delta_phi * dir)));
        % Values for PSOS:
```

```
31          p_list(n/2) = p_new;
32          s_list(n/2) = s_new;
33
34      else
35          % New values for the new disk
36          if imag(z(n-1)) < 0 % Checks if ray is in the lower half of
                disk
37              theta = asin(sin(theta1)*n1/n0); % Angle out of the disk
38              [z_new, p_new, s_new, dir_new] = new_values(z(n-1), theta,
                    dir, r, d);
39              if z_new == 0 % If the ray leaves the system
40                  break
41              end
42              z(n) = z_new;
43              theta0 = abs(asin(p_new));  % updating incident angle
44              phi = s_new*r*pi;           % defining new phi
45              dir = dir_new;              % updating direction
46          else
47              % Ray leaves the system
48              break
49          end
50      end
51  end
```

A.4 new_values.m

```
%% Finds new values of intersection at the next disk in the array
%
% This program calculates the values for the ray at the new disk. In
    the
% case of the ray leaving the system, the program will return 0 if ray
% leaves the system

function [z_new, p, s, dir] = new_values(z, theta, dir, r, d)

%% Changing polar coordinates to cartesian and determining angles

x = real(z);
y = imag(z);

z_new = 0; % Standard value if ray leaves system
p = 0;
s = 0;
alpha = acos(abs(y/r));
y_angle = alpha + theta; % The angle of the ray from the -y direction

%% Returns the p- and s- value of the new disk
% Calculations for the left quadrant
if x < 0
    % Determine x-direction:
    x_dir = -1;
    if dir == -1
        if theta < alpha
            y_angle = alpha - theta;
        else
            y_angle = theta - alpha;
```

```
30              x_dir = 1; % The angle of the ray will be in positive x-
                    direction
31          end
32      end
33      m = abs(tan((pi/2) - abs(y_angle)))*-x_dir;
34      c = (-m*x)+y+(2*r)+d;
35
36      if abs(m) < 10^15   % Loophole for approximately vertical rays
37          [new_x, new_y] = intersection(m,c,r);
38      else
39          new_x = x;
40          new_y = abs(y);
41      end
42
43      if new_x ~= 0 || new_y~=0
44          if new_x < 0
45              phi = abs(atan(new_x/new_y))+(pi/2);
46          else
47              phi = abs(atan(new_y/new_x));
48          end
49          z_new = r*exp(1i*phi);
50          s = r*phi/pi;
51          if x_dir == 1
52              if phi - (pi/2)<y_angle
53                  dir = 1;
54                  p = sin(y_angle-phi-(pi/2))*dir;
55              else
56                  dir = -1;
57                  p = sin(phi-(pi/2)-y_angle)*dir;
58              end
59          else      % x_dir == -1
60              dir = -1;
```

```
61              p = sin(phi-(pi/2)+y_angle)*dir;
62          end
63      end
64  % Calculations for the right quadrand
65  elseif x > 0
66      % Same as x < 0, but reverted
67      x_dir = 1;
68      if dir == 1
69          if theta < alpha
70              y_angle = alpha - theta;
71          else
72              y_angle = theta - alpha;
73              x_dir = -1;
74          end
75      end
76      m = abs(tan((pi/2)-abs(y_angle)))*-x_dir;
77      c = (-m*x)+y+(2*r)+d;
78
79      if abs(m) < 10^15   % Loophole for approximately vertical rays
80          [new_x, new_y] = intersection(m,c,r);
81      else
82          new_x = x;
83          new_y = abs(y);
84      end
85      if new_x ~= 0 || new_y~=0
86          if new_x >= 0
87              phi = abs(atan(new_y/new_x));
88          else
89              phi = abs(atan(new_x/new_y))+(pi/2);
90          end
91          z_new = r*exp(1i*phi);
92          s = r*phi/pi;
```

```
93          if x_dir == -1
94              if ((pi/2)-phi) < y_angle
95                  dir = -1;
96                  p = sin(y_angle-(pi/2)+phi)*dir;
97              else
98                  dir = 1;
99                  p = sin((pi/2)-y_angle-phi)*dir;
100             end
101         else % x_dir == 1
102             dir = 1;
103             p = sin(y_angle+(pi/2)-phi)*dir;
104         end
105     end
106 % In the case of x = 0
107 else
108     z_new = r*exp(1i*pi/2);
109     s = 1/(2*r);
110     p = sin(theta)*dir;
111
112 end
```

A.5 intersection.m

```
%%% Calculates the intersection of the ray and next disk
%
% In the case of the ray leaving the system the output coordinates is
    0,0
%
function [x1,y1] = intersection(m, c, r)

A = 1+m^2;
B = 2*m*c;
C = c^2 - r^2;

if B^2-(4*A*C) > 0       % Two real solutions
    x1 = ((-B+sqrt(B^2-(4*A*C)))/(2*A));
    x2 = ((-B-sqrt(B^2-(4*A*C)))/(2*A));
    y1 = (m*x1) + c;
    y2 = (m*x2) + c;

    % Choosing the correct intersection point
    if y1>0 && y2>0
        if m < 0
            if x1>x2
                x1 = x2;
                y1 = y2;
            end
        else
            if x1<x2
                x1 = x2;
                y1 = y2;
            end
        end
```

```
30      else
31          if y1 < 0
32          y1 = y2;
33          x1 = x2;
34          end
35      end
36
37  elseif B^2-(4*A*C) == 0 % One real solution
38      x1 = (-B+sqrt(B^2-(4*A*C)))/(2*A);
39      x2 = ((-B-sqrt(B^2-(4*A*C)))/(2*A));
40      if ~isreal(x1)
41          x1 = x2;
42      end
43      y1 = sqrt(r^2-x1^2);
44
45  else                        % No intersection
46      x1 = 0;
47      y1 = 0;
48  end
```

A.6 test_plot.m

```
%
% This script was used for testing the trajectory of rays and show the
% trajectory of a ray over a larger amount of disks
%

%% Input values

s0 = 0.4;        % Start position
p0 = 0.4*1.7;    % start momentum

no_of_points = 36;        % number of calculated points per simulation
no_of_simulations = 1;    % Number of simulated rays

n0 = 1.0;                  % surrounding refractive index
n1 = 3;                    % refractive index of disk
r = 1;                     % radius of disk
d = 0.4;                   % distance between the disks

%% disk coordinates

unit_circle = 0:0.02:2*pi;

disk_x = r*cos(unit_circle); % x-coordinates for the disk
disk_y = r*sin(unit_circle); % y-coordinates for the disk

%% Plotting the rays and disks

for i=1:no_of_simulations
    if i>1
        figure
```

```
31      end
32      rng('shuffle');
33      %s0 = (rand*0.2)+0.4;
34      %p0 = rand*0.05;
35      [z, s, p] = disk(s0,p0,n0,n1,no_of_points,r,d);
36      for n = 2:2:length(z)
37          plot ([real(z(n-1)) real(z(n))], [imag(z(n-1))-n+2-(((n-2)/2)*d
                ) imag(z(n))-n+2-(((n-2)/2)*d)], 'r');
38          hold on
39          %axis([-1 1 -inf 1])
40      end
41
42      %Plotting the disks:
43
44      for x = 1:length(z)/2
45          for j = 1:length(unit_circle)
46              plot(disk_x,disk_y - (2*r*x)+2 -((x-1)*d),'k');
47              %axis
48              grid on
49              hold on
50          end
51      end
52
53      %Plotting |p|-graph
54
55      figure
56      plot(abs(p))
57  end
```

Norges miljø- og biovitenskapelig universitet
Noregs miljø- og biovitskapelege universitet
Norwegian University of Life Sciences

Postboks 5003
NO-1432 Ås
Norway